This is a preprint, the final version is subject to change, of the American Mineralogist (MSA)
Cite as Authors (Year) Title. American Mineralogist, in press.
(DOI will not work until issue is live.) DOI: http://dx.doi.org/10.2138/am-2017-5971

Revision 2

Mineralogical and compositional features of rock fulgurites: a record of lightning effects on granite

Chiara Elmi[1*], Jiangzhi Chen[1], David Goldsby[1], Reto Gieré[1]

[1]*Department of Earth and Environmental Science, University of Pennsylvania, 240 S. 33rd Street, Philadelphia, Pennsylvania, 19104-6313, U.S.A.*

*Corresponding author: Chiara Elmi, chiarael@sas.upenn.edu

Abstract. Fulgurites are a naturally occurring glass formed when sand, rock, or soil is struck by atmospheric electrical discharges (lightning). The aim of this paper is to provide insights into the conditions occurring in rocks during the lightning strike. Rock fulgurites collected from Mt. Mottarone, Baveno (Piedmont, Italy) have been investigated to assess the mineralogical and compositional changes occurring in granite due to a lightning strike. X-ray powder diffraction showed that the samples represent the dominant granitic rock type of the Baveno massif, the so-called "Pink Baveno". Fulgurite coats the surface of the granite as a brown-black, glassy to very fine-grained porous layer. Powder diffraction data for the fulgurite reveal the presence of cristobalite and quartz crystals in a glass matrix, suggesting that temperature exceeded ~1700 ºC at near atmospheric conditions, assuming thermodynamic equilibrium. Electron probe microanalysis of the glass revealed that it is mainly composed of SiO_2 and Al_2O_3 and that it has a porosity of 5-7 area% in the studied zones. The presence of the amorphous phase indicates that the abrupt electrical (Joule) heating of the rock surface yielded high temperatures, producing a thin melt layer on the surface which then cooled adiabatically. Idealized physical model was developed to simulate the effects of Joule heating and subsequent thermal conduction close to the rock surface during and

after a lightning strike. The quantity of organic matter in the glass, obtained via Elemental Analyzer, suggests that rapid quenching of the melt trapped NO_x and CO_x gases produced during heating. Raman spectroscopy revealed the presence of polyaromatic hydrocarbon molecules, which, combined with the Elemental Analyzer data, suggest that organic matter was pyrolysed at around 300-350 ºC and then trapped in the glass matrix of the studied rock fulgurites.

Key Words – lightning, rock fulgurites, mineralogy, compositional features, physical models

INTRODUCTION

Lightning is a transient, high-current discharge occurring within a thundercloud, between clouds, or between a cloud and the ground whose path may be many kilometers long (Uman and Krider, 1989a; Uman and Krider, 1989b). Christian et al. (2003) estimated the frequency of lightning across the globe at 1.2×10^9 flashes per year. The majority (~90%) of these lightning flashes occur over continental landmasses as opposed to the open ocean (Lay et al., 2007). Any type of clouds can potentially cause lightning or some related form of electrical discharge, as can snowstorms, volcanic eruptions, and dust storms (Uman and Krider, 1989a).

Over half of the flashes occur within clouds, known as intra-cloud (IC) discharges. Cloud-to-ground (CG) lightning, although accounting for only about one-third of lightning flashes (Rakov, 1999), are the most studied because of their impact on human life (Uman and Krider, 1989a). Each CG lightning strike involves an energy of 10^9–10^{10} J, most of which is consumed to produce thunder, hot air, light, and radio waves (Rakov, 1999; Saikia et al., 2008). On the ground, typical peak currents can reach 30 kA, and their half-life is about 50 μs (Uman and Krider, 1989a). The term fulgurite (from the Latin *fulgur*, lightning) describes a naturally occurring glass formed when sand, rock, or soil is impacted by CG lightning strikes. The occurrence of fulgurites has also been documented on man-made structures (*e.g.*, Martin Crespo et al., 2009).

Pasek et al. (2012) classified fulgurites into four types based on morphology and mineralogical composition. Type-I fulgurites are sand fulgurites consisting of hollow glass tubes with sand adhering to the outside, formed when lightning strikes a body of sand; type-II fulgurites are clay fulgurites, consisting of thick, melt-rich walls; type-III fulgurites are caliche fulgurites, consisting of thick, glass-poor walls; and type-IV fulgurites are rock fulgurites, formed when lightning strikes the surface of rocks, appear mostly as thin glassy crusts, which may be relatively low in silica, and exhibit a wide variety of colors depending on the composition of the rock (Essene and Fisher, 1986; Clochiatti, 1990; Grapes and Müller-Sigmund, 2009; Martin Crespo et al., 2009; Carter et al., 2010b).

Although a fulgurite specimen that may be as old as 15 ky was collected in the Libyan Desert (Navarro-Gonzalez et al., 2007), fulgurite materials are typically geologically young and are sometimes collected within days of formation. They commonly contain non-melted precursor minerals cemented into the fulgurite glass. Shock, while proposed to occur in association with fulgurites, remains controversial, since fulgurites typically do not contain high-pressure SiO_2 polymorphs or quartz exhibiting planar deformation features. However, there is some evidence that minerals within fulgurite (Carter et al., 2010a; Carter et al., 2010b; Ende et al., 2012), or in the underlying rock (Gieré et al., 2015), display signatures of shock, similar to those reported for rocks affected by meteorite impacts (*e.g.*, French and Koeberl, 2010). The formation of fulgurites is accompanied by mineralogical and sometimes compositional changes, and may record information about the environment (*e.g.*, fulgurites in the Libyan Desert preserve paleoclimate information) in which they were formed (Switzer and Melson, 1972; Sponholz et al., 1993; Sponholz, 2004; Navarro-Gonzalez et al., 2007).

Determination of the range of conditions produced by lightning in Earth and engineering materials (*e.g.*, in wind mills and transmission towers) is an important scientific goal of this study. The need to transport energy over longer distances is pushing manufacturers to research, develop, and produce components capable of operating at ever-higher voltages and to develop materials able

to preclude damage to power lines and, eventually, power outages. In these applications, the quality of the insulation to protect electrical power lines from CG lightning strike has become a crucial design element. The mineralogical and chemical properties of rock fulgurites can provide insights into the conditions occurring during lightning strikes, and aid in the design of better lightning protection systems in industrial and planetary applications (*e.g.,* in aircraft and space vehicles).

Pasek and Hurst (2016) provided a means of directly determining the energy of a lightning strike in CG strikes on fine quartz sand. These authors observed sand fulgurites that were formed in a homogenous target and had a specific morphology. The lack of information on the formation of rock-fulgurites can be attributed to the heterogeneity of the rock target and the resulting complexity of the phenomena associated with lightning strikes, as well as the challenges faced when considering mineralogical and compositional changes in such a heterogeneous material under highly non-equilibrium conditions. The aim of this paper is to provide insights into the conditions occurring during lightning strikes on rocks with qualitative and quantitative mineralogical and chemical data for rock fulgurites. Moreover, idealized physical model was developed to simulate the effects of Joule heating and subsequent thermal conduction close to the rock surface during and after a lightning strike.

GEOLOGICAL SETTING

Six samples of rock fulgurite, which appears as a dark brown-black layer on the surface of pink granite (Fig. 1), were collected near the top of Mount Mottarone (45º52’18”N/8º26’44.6”E, 1327 m above sea level) from a well-exposed, N–S trending ridge that forms steep cliffs (Fig. 1a). The Baveno-Mottarone granitic pluton, dated at ~270 m.a. (Jager and Faul, 1959), is part of the Baveno-Mottarone massif, located on the western shore of Lago Maggiore and elongated from SSW to NNE in the Western Alps of north-western Italy, near the town of Baveno.

The Baveno-Mottarone massif is geologically located in the “Serie dei Laghi” (also known as the Strona–Ceneri Zone), which is adjacent the Ivrea–Verbano Zone. These two lithostratigraphic belts

have been the subjects of intense research activity for more than 45 years following the discovery that a strong positive gravity anomaly indicative of dense mantle and lower crustal rocks is associated with the Ivrea–Verbano Zone (Sinigoi et al., 2016). The Ivrea–Verbano Zone constitutes the lower part of the section. Within it, the so-called Kinzigite Formation, a pre-Permian volcano-sedimentary sequence metamorphosed in amphibolite to granulite facies (Zingg, 1983), was intruded by an 8 km-thick Mafic Complex, which is composed of mostly gabbroic rocks (Rivalenti et al. 1975; Rivalenti et al. 1984). The "Serie dei Laghi" constitutes the upper part of the section and is comprised of lower amphibolite-facies schists and gneisses (Caironi, 1985; Boriani et al., 1988; Boriani et al., 1990) intruded by granite plutons referred to as the "Graniti dei Laghi". Ultramafites and metagabbros form small lenses near the contact of the "Serie dei Laghi" and the Kinzigite Formation (Sinigoi et al., 2016).

Gallitelli (1937) and Boriani et al. (1988) observed the presence of different granitic facies in the Mottarone-Baveno pluton: medium- or medium-to-fine-grained red, pink, and white granites, micro- and hetero-granular granite, and granodiorite. The miarolitic granite, with a small percentage of red granite, constitutes the upper layer of the Mottarone-Baveno pluton (Dino et al., 2012). The pink granite facies ("Pink Baveno") is a well-known ornamental stone, which has been quarried in the district over the last centuries (Sandrone et al., 2004), as is the white granite, known as the Mont'Orfano and the Alzo-Roccapietra granites (Bugini et al., 2000). The transition from the white to the pink granite is mainly chromatic. The pink color of granitic rocks is due to the presence of numerous open pores in K-feldspar, up to several hundred nanometers in cross-section, which contain rosettes or needles of hematite (Putnis et al. 2007).

MATERIALS AND METHODS

X-ray powder diffraction

X-ray powder diffraction (XRPD) was used to identify the mineralogical composition of both the bulk granite and the fulgurite (the black layer, see Fig. 1b) on the surface of the rock. X-ray patterns

were collected at room temperature using a PANalytical X'Pert diffractometer equipped with an X'Celerator detector, and CoKα radiation (40 kV/40 mA). Cobalt radiation was chosen to avoid fluorescence between Fe-bearing minerals and Cu radiation. The incident beam optical module PANalytical Bragg-Brentano^{HD} was used to improve the peak-to-background ratio and increase intensity in measured spectra.

Bulk analyses of the granite were carried out with spinner-mode analysis, a 2θ scan range between 5° and 80°, a step size of 0.02° 2θ, a divergence slit of 0.125°, and anti-scatter slits of 0.5°. The fitted peak width for collected data was about 0.01º 2θ.

The rock fulgurite was gently removed from the rock with a razor blade, and the resulting powder was sieved to <38 μm, and then ground with an agate mortar and pestle. Samples were filled into Mark-tubes (Lindemann special glass, with a nominal outside diameter of 0.3 mm and a wall thickness of 0.01 mm) for capillary spinner-mode analysis. Data were collected with a scan range between 5 and 100° 2θ, a step size of 0.02° 2θ, a divergence slit of 0.125°, and anti-scatter slits of 0.0625°. The fitted peak width for collected data was about 0.01º 2θ. Quantitative mineralogical analyses and determination of the content of amorphous material with the external-standard method (the K-factor method after O'Connor and Raven (1988)) were performed using PANalytical's HighScore Plus version 4.5 software (Degen et al., 2014). Pure crystalline Al_2O_3 (NIST SRM 676a) was chosen as an external standard and was analyzed under the same instrumental conditions as the samples.

X-ray fluorescence

Bulk analysis of granite was performed by SGS Mineral Services Canada Inc. according to their laboratory procedures GO XRF76V (borate fusion, reported detection limit of 0.01 wt%) and GO XRF77B (pyrosulfate fusion, reported detection limit of 0.01 wt%), followed by X-ray fluorescence (XRF) analysis. The sample was pulverized and then sieved (mesh number = 200, sieve size = 74 μm) prior to analysis. The sample aliquot designated for XRF analysis was 5 g.

156

157 *Optical microscopy and environmental scanning electron microscopy*

158 Polished thin sections (~30 μm thick) of samples Motta 5, Motta 6, and Motta 7 from Mt.
159 Mottarone were investigated with a petrographic microscope in plane-polarized and crossed-
160 polarized light. Thin sections of samples Motta 5 and Motta 7 were then studied by environmental
161 scanning electron microscopy (ESEM) using an FEI Quanta-600 in the Singh Center for
162 Nanotechnology at the University of Pennsylvania. Secondary electron (SE) and backscattered
163 electron (BSE) images were collected, and energy-dispersive spectroscopy (EDS) was used to
164 determine the qualitative chemical composition of the minerals in the fulgurite layer (with a beam
165 spot diameter of 2 μm). The images were collected in low vacuum (about 10^{-4} Torr) at an
166 accelerating voltage of 15 kV.

167

168 *Electron probe microanalysis (EPMA)*

169 The quantitative chemical compositions of minerals in the granite substrate and in the fulgurite
170 glass, as well as of the glass itself, were estimated on three selected thin sections (Motta 5, Motta 6,
171 and Motta 7). Analyses were performed with a Cameca SX 100 electron microprobe equipped with
172 five wavelength-dispersive spectrometers and one energy-dispersive spectrometer in the
173 Department of Earth, Environmental and Planetary Sciences at Brown University.

174 The following operating conditions were applied to analyze the fulgurite glass composition: an
175 accelerating voltage of 15 kV, a sample current of 10 nA, 30 s on peak, 15 s on backgrounds on
176 either side of the peaks, and a wide beam diameter of 5 μm. The following standards were used:
177 orthoclase (K), albite (Na), Rockport fayalite (Fe), synthetic pantelleritic glass (Si, Al), diopside
178 glass (Ca), synthetic olivine (Mg), rutile (Ti), Ni metal (Ni), rhodonite (Mn), barite (Ba), synthetic
179 berlinite (P), pyrite (S), and richterite (F). The raw data were corrected using the PAP procedure
180 (Pouchou and Pichoir, 1991). Analyses of more than sixty points on fulgurite glass were made to
181 produce a statistically significant average along the layer.

EPMA was also performed on plagioclase and alkali feldspar crystals in the granite. The operating conditions for minerals in the bulk rock were identical to those for the glass (see above). The following standards were used: orthoclase (K, Si), anorthite (Ca, Al), albite (Na), rutile (Ti), Rockport fayalite (Fe), synthetic olivine (Mg), and barite (Ba). Analyses of more than nine points on each crystal showed sample homogeneity.

Total organic carbon and nitrogen Elemental Analyzer

A COSTECH-4010 micro Elemental Analyzer (EA) combined with a gas chromatographic technique was used to determine total organic carbon and nitrogen in the rock fulgurite powder. Each sample was placed in a tared tin capsule (diameter = 5 mm, height = 9 mm) and weighed using a microbalance. All samples were dried at 80 °C prior to analysis.

The combustion temperature was set to 1700 °C, the oxygen flow rate was 100 mL/min and atropine (N = 4.84 wt% and C = 70.56 wt%) was used as an organic analytical standard. Five samples of atropine, varying in weight from 0.3 mg to 2.3 mg, were used to construct the calibration curve. The EA software compared the C and N peaks of the sample to those of atropine after calibration.

Raman Spectroscopy

A thin section of sample Motta 7 was selected for Raman spectroscopic analysis. All spectra were collected at the Singh Center at the University of Pennsylvania using a ND-MDT Nano-Raman NTEGRA Spectra equipped with a conventional Olympus IX71/IX81 optical microscope, with a 100X objective to focus the laser spot. The maximum power of the laser was 150 mW. All measurements were made at 25 °C. Spectra were collected in inverted mode with an Andor CCD (charged-coupled device) detector. Sample areas as small as 1 μm^2 were analyzed with an integration time of 5 s. Three acquisitions per spot were stacked to improve the signal-to-noise ratio. The excitation source was the 514.5 nm green light line of an Ar^+ laser. The spectrometer was

fitted with a holographic notch filter (532 nm) and grating (600 g/mm), and was controlled using the software NOVA30.

RESULTS

Characterization of the granite

The mineralogical composition of the bulk granite was analyzed via XRPD and a representative XRD pattern is shown in Fig. 2. The granite consists of quartz, plagioclase, K-feldspar, and micas, mostly biotite (Table 1). The chemical composition of a fresh rock sample, collected at the fulgurite site and characteristic of the rocks exposed at the outcrop, shows that it is a typical granite (Table 2). The studied rock samples represent the dominant granite type of the Baveno massif, the so-called "Pink Baveno". Most analyzed trace elements, including Ba, were not detectable.

Chloritized biotite phenocrysts are observed via optical microscopy and, in hand specimen, appear dark green in color with a dull luster. XRPD diagrams for some of the samples (Motta 3 and Motta 4) showed a *d*(001) peak near 14 Å, consistent with chlorite (Table 1).

Under crossed polarizers, albite lamellar twinning is visible in most plagioclase crystals. The crystals have undergone intense secondary alteration. The average chemical composition of plagioclase is $Ab_{97.55}An_{1.02}Or_{1.43,}$ that of alkali feldspar is $Ab_{4.70}An_{0.00}Or_{95.30}$, *i.e.*, K-feldspar (orthoclase, see Table 3). K-feldspar typically occurs as lightly pink euhedral crystals ranging in size from 1 to more than 3 cm and thus, is easily visible in hand specimens. An advanced stage of myrmekite replacement of K-feldspar crystals was observed in the optical microscope. Quartz crystals are unaltered and in some cases contain fluid inclusions. The quartz grains underlying the fulgurite layer are finely cracked (Figs. 3, 4a,c,f).

Characterization of the fulgurite

Optical microscopy showed that the rock fulgurite from Mottarone coats the pink granite as a brown-black, glassy to very fine-grained layer (Figs. 3, 4a,b). The fulgurite layer contains tiny,

optically unidentifiable crystals as well as small opaque spherical objects (Fig. 4b). In BSE images, the latter appear as spheres (average diameter about 1 μm) with a very bright gray-scale contrast (Fig. 4c,d). The ESEM-EDS data showed that these spheres were FeO- and SiO_2-rich, but unfortunately, they were too small for EPMA.

ESEM investigations revealed the ubiquitous presence of voids in the fulgurite layer (Figs. 4c, e,f). Values of the porosity of the fulgurite layer, obtained from ESEM micrographs using *ImageJ* (Schneider et al., 2012), are 7 area% in Figure 4e and 5 area% in Figure 4f. The average pore dimension is 0.9 μm in Figure 4e and 1.3 μm in Figure 4f.

In BSE images, the fulgurite layer in Motta 5 (Fig. 4c,f) and Motta 7 (Fig. 4d) further exhibited bright spots (≤ 2 μm in size) inside some of the voids. These grains were determined to be barite ($BaSO_4$) by ESEM-EDS, but unfortunately they were too small for EPMA.

BSE images of samples Motta 5 and Motta 7 revealed the presence in the fulgurite layer of rounded grains with a higher contrast than the surrounding matrix (Fig. 4c,d,e,f). The shape of these grains, in combination with SEM-EDS and EPMA data (not shown), indicates that these phases represent partially melted relics of quartz, K-feldspar (orthoclase), and plagioclase (albite). Tiny (≤ 2 μm) crystals of ilmenite, rutile, and epidote were also observed in the fulgurite glass of Motta 5, and a crystal of magnetite was detected in the Motta 7 fulgurite; none of these crystals were large enough for EPMA.

XRPD analysis allowed for determination of the mineralogical composition of the fulgurite layer in the studied samples. The data revealed the presence of an amorphous phase (66.6 – 98.1 wt%, Table 4) and quartz (probably a residual phase) in all six fulgurite samples, as well as cristobalite in five samples (Fig. 5, Table 4). The XRPD data further showed that albite is present in three of the fulgurite samples (Motta 5, Motta 6, Motta 7; Fig. 5d,e,f). These results confirm that the rounded grains observed in the glass matrix via ESEM (see above and Fig. 4c,d,e,f) most likely represent residual, partially melted crystals of the granite substrate. The broad *d*(001) peak at about 14 Å

observed via XRPD in fulgurite sample Motta 5 (Fig. 5d) is consistent with an expanded clay mineral such as vermiculite.

The amorphous phase, studied and quantified via XRPD, is composed mainly of SiO_2 and Al_2O_3 in the analyzed areas (Table 5). The SiO_2 and Al_2O_3 contents of this fulgurite glass, however, are considerably lower than those in the granite substrate (see Table 2). Even more depleted relative to the original granite are the Na_2O and K_2O contents of the glass (*cf.* Tables 2 and 5). The compositional analyses of the fulgurite layer showed very low totals (Table 5). Low totals are a typical feature of fulgurite analyses and result from microporosity as well as the presence of water, gases, and carbon within the analysis volume of the EPMA (Grapes and Müller-Sigmund, 2009; Gieré et al., 2015).

ESEM investigations showed that micas, although present in the original granite (Table 1), do not occur in the fulgurite glass layer. A biotite crystal, detected with the optical microscope at the boundary between the granite substrate and the fulgurite, was studied using ESEM, and the SE images show that the top layers of the biotite were melted (Fig. 6).

Organic matter in fulgurite layer

The data for the total organic matter content in the fulgurite layer (Table 6) demonstrate high quantities of both carbon (up to 7 wt%, expressed as CO_x) and nitrogen (up to 0.87 wt%, expressed as NO_x) species. These values explain, at least partly, the low totals obtained by EPMA for the fulgurite glass (see above and Table 5). The NO_x and CO_x contents display a strong positive correlation (Fig. 7).

Micro-Raman measurements in the range 300 to 2700 cm^{-1} were performed along the Motta 7 fulgurite layer, a specimen bearing representative NO_x and CO_x contents (Table 6). The Raman spectra, collected in four different areas of this specimen, revealed both sharp and weak bands, suggesting that some of the carbon present in the glass matrix is composed of polyaromatic hydrocarbon molecules (Fig. 8).

Alkene C=C conjugated with –N exhibits a strong absorption in the region 1680-1630 cm^{-1} (Socrates, 2001), and thus the peak at 1633 cm^{-1} in Fig. 8a and 8d can be ascribed to the tri-substituted alkene functional group >C=C–N<. The conjugated cyclic system containing C=N has, due to the stretching vibration, a band of variable intensity in the region 1660-1480 cm^{-1} (Socrates, 2001). According to Socrates (2001), the peak at 1470 cm^{-1}, seen in Fig. 8a, can be ascribed to the oxime group >C=N–, whereas the peaks at 853 cm^{-1} (Fig. 8a) and 836 cm^{-1} (Fig. 8b) can be ascribed to monomer SiO_4 units (Carter et al., 2010a). The peak at 540 cm^{-1} can be ascribed to alkene C=C conjugated to an aromatic group and to cyclic alkenes (Socrates, 2001), whereas the peak at 780 cm^{-1} (Fig. 8b) can be interpreted to be derived from the scattering of cristobalite microlites (Arias et al., 2006). The peak at 1402 cm^{-1} (Fig. 8c) can be attributed to the hydrocarbon functional group of vinylidene, >C=CH_2 (Socrates, 2001). The peak at 1622 cm^{-1} (Fig. 8c), like that at 540 cm^{-1} (Fig. 8b), can be ascribed to alkene C=C conjugated to an aromatic group and to cyclic alkenes (Alajtal et al., 2010; Socrates, 2001), and the peak at 1357 cm^{-1} (Fig. 8d) can be ascribed to C–C stretching (Alajtal et al., 2010). The broad peaks at 2030 and 2300 cm^{-1} in all spectra (Fig. 8) are consistent with water molecules in the glass matrix (Carabatos-Nedelec, 2001).

Idealized physical models of thermal conduction during and after the lightning strike

An idealized physical model was developed to simulate the effects of Joule heating during and after the lightning strike on a granite and to estimate the area of burnt organic matter. The granite is heated not only from the heat diffused from the lightning channel where the peak temperature is estimated to be in the range 1-3 $\times 10^4$ K (Uman, 1969) to 10^5 K (Uman, 1964) using gas plasma models, but also from the electrical current passing through the rock when lightning strikes. The thermal diffusivity κ of granite is 0.913 mm^2/s (Eppelbaum et al., 2014), and the lightning strike lasts typically for $\Delta t \sim 50$ μs (Uman and Krider, 1989b). The length scale of the region affected by

thermal diffusion after the lightning strike is $\sqrt{\kappa \Delta t} \approx 7$ μm, much smaller than the region affected by Joule heating, as shown below.

The top surface of the rock is weathered, and, due to moisture in the weathered layer, the surface can have a value of electrical conductivity σ that is 10–50 times larger than the value of the electrical conductivity σ_0 (~10^{-3} S/m) of the underlying rock (Olona et al., 2010). However, given the fact that the weathered layer has a thickness < 1 mm, which is negligible compared to the thickness of the rock, which is at least several tens of centimeters, the electrical and temperature fields do not deviate significantly from those for homogeneous granite. The penetration of lightning in rock fulgurites is also limited to the top surface of the rock, in stark contrast with the long tubular structures observed in sand fulgurites. Thus, a simple cylindrical diffusion model (Carter et al., 2010b; Pasek et al., 2012) is not applicable for modeling of rock fulgurites.

The granite is assumed to be an axisymmetric semi-infinite half space, with the z axis pointing from the surface toward the interior of the rock, and $\vec{r}$ is the position vector of any point from the hit point. When the lightning is treated as a point source of current of intensity I hitting the rock vertically, the temperature $T(\vec{r}, t)$ caused by the electrical field $\vec{E}(\vec{r}, t)$ can be modeled as

$$\frac{\partial T}{\partial t} = \kappa \nabla^2 T + \frac{\sigma E^2}{\rho C}$$

where the density ρ is ~ 2800 kg/m^3 (Frederikse, 2004), and the specific heat C is ~790 J/(kg K) (Eppelbaum et al., 2014). The electrical field is

$$E = \frac{I}{2\pi\sigma_0 r^2}$$

where r is the distance from the lightning hit point. Dimensional analysis suggests that when $I \gg \kappa\sqrt{\rho C \Delta t \sigma_0 \Delta T}$, thermal diffusion can be ignored during the lightning strike. For a typical lightning strike with I~ 10 kA (Uman and Krider, 1989b), the surface temperature rise after the lightning can be estimated as

$$T \approx \frac{\sigma_0 E^2 \Delta t}{\rho C} + T_a,$$

where T_a is ambient temperature (25ºC). Figure 9 shows how the instantaneous radial component of the electrical field (blue curve) and the temperature (red curve) vary with distance from the hit point. The temperature rise on the granite surface was indicated by the burning of organic materials there. Considering the surface ignition temperature of woody materials to be around 300 ºC (White and Dietenberger, 2001), labeled by the black horizontal dashed line in Figure 9, the area of the burnt organic matter can be estimated. The figure suggests that the area of burnt organic matter extends to a radius of about 13 cm, consistent with field observations.

DISCUSSION

The existence of fulgurites provides direct evidence that the chemical and mineralogical composition of the target rock is altered due to the heat generated by lightning discharges. Fulgurite formation is a highly energetic process with an energy density of the same order of magnitude as impact events, especially micrometeorite impacts (Bouška and Feldman, 1994; French and Koeberl, 2010; Kenkmann et al., 2014). Both processes cause a rapid rise in temperature followed by rapid isentropic cooling.

The presence of the glass on the surface of the pink Baveno granite on Mt. Mottarone, as evidenced by field observations (Fig. 1), optical microscopy (Fig. 4a,b), ESEM (Fig. 4c,d,e,f), and XRD (Fig. 5), indicates that the abrupt heating of the rock surface yielded temperatures that were high enough to produce a thin melt layer on the surface, which then cooled adiabatically. The morphology of quartz, plagioclase, and K-feldspar crystals observed within the fulgurite by ESEM (Fig. 4c,d,e,f) was rounded, suggesting partial melting and subsequent rapid cooling.

Rakov (1999) observed that the peak temperature in a rock struck by lightning depends on the target rock composition and the presence or absence of water. The melting temperature of dry granite at ambient pressure is 1215–1260 °C, but it is strongly reduced in the presence of water,

down to 950 °C (Holland and Powell, 2001). However, the presence of cristobalite detected via XRD (Fig. 5) would indicate melting temperatures above ~1700 ºC and pressures near atmospheric, if thermodynamic equilibrium were obtained. Such high temperatures were indeed achieved near the lightning strike point in the studied granite, as indicated by temperature modeling (Fig. 9).

Considering the chemical analyses reported in Table 5 and according to Frost et al. (2001), the lightning strike on the Baveno-Mottarone granite produced a fulgurite glass of peraluminous granitic composition, with an average ASI of 1.5(2). The low concentrations of Na_2O, CaO, and K_2O in the glass suggest that alkali and alkaline earth elements were liberated from feldspars during heating. The quantity of P_2O_5 detected in the fulgurite glass using EPMA (Table 5) was observed to be higher than in the substrate (Table 2). The relatively high amounts of P_2O_5 in fulgurite glass point to the possible presence of organic matter on the granite surface at the time of the lightning strike, consistent with the high CO_x and NO_x contents. Relatively high phosphorus content was also found in rock fulgurites from other localities (Grapes and Müller-Sigmund, 2009; Pasek and Block, 2009; Pasek et al., 2012; Gieré et al., 2015).

Natural glasses are formed from a liquid state by supercooling, or as condensate from a rapidly cooled sublimate (Bouška and Feldman, 1994). The quantity of organic matter in the glass (Table 6) suggests that rapid quenching of the melt trapped NO_x, and CO_x gases produced during heating. The strong positive correlation between NO_x and CO_x in the studied rock fulgurite (Fig. 7) supports the hypothesis that these species might be derived from organic matter (*e.g.*, lichen, leaves, pollen, roots), present on the rock surface before the lightning strike, which was burnt during the strike. The N/C ratios (Table 6) are close to those observed by Adamo et al. (2008) for burnt lichens, suggesting that much of the carbon and nitrogen present in the fulgurite is related to microorganisms on the pink granite before the lightning strike. Moreover, field observations revealed the presence of lichen and algal biofilms on the pink granite in close proximity to the site where the fulgurite samples have been recovered (Fig. 1b). The rounded cavities in the fulgurite glass (Fig. 4c,e,f) can be related to gases (*e.g.*, H_2O vapor, NO_x, CO_x) escaping during the lightning

strike. The Raman spectra, collected in four different areas of Motta 7, revealed both sharp and weak bands, suggesting that much of the carbon present in the matrix is composed of polyaromatic hydrocarbon molecules (Fig. 8), which are often considered as products of incomplete combustion (*e.g.*, Garra et al., 2015). The presence of alkene and oxime functional groups trapped in the fulgurite glass indicates extremely reducing conditions, which may reflect the conditions during the quenching of the melt. In oxidizing environments water vapor and carbon dioxide are produced from burnt organic matter at about 300 ºC (White and Dietenberger, 2001). During ignition tests, White and Dietenberger (2001) observed that flammable volatiles, water vapor, and other non-combustible gases (*i.e.*, CO_2, formic acid, and acetic acid) are produced vigorously at 300°C and that all components of organic matter end their volatile emissions at around 450°C. According to the results obtained in this study with Elemental Analyzer and by Raman spectroscopy, organic matter could be pyrolysed at ~300-350 ºC and then trapped in the fulgurite glass. Further investigations on these organic reduced phases should be carried out in future experiments in order to better clarify the formation of these molecules.

The idealized physical model reveals that while the lightning strike only lasts about 50 μs, the high electrical current, up to 10 kA, easily generates enough heat to burn the surficial organic matter. The modeling showed that with a thin, highly-conductive weathered layer on the surface, the effect of Joule heating is strong near the surface and close to the lightning hit point. The effects of the shock wave, which results from the sudden expansion of heated air around the lightning channel, were neglected. The model treats the lightning as a point source, yielding an electrical field strength in the vicinity of the lightning strike of more than 10^{11} V/m. This value exceeds the breakdown electrical field strength for the burnt organic material (O'Dwyer, 1969) on the surface, and the resulting temperature is > 10^5 ºC, if all the thermal and electrical properties of the rock remained constant during the process. In fact, the electrical conductivity can be affected by multiple factors, including decreased moisture content during the heating, and increased electron activity due to partial melting (Olhoeft, 1981). These effects were mostly confined to the very thin surface layer

406 near the strike point, and the strong decay of the electrical ($E \propto r^{-2}$) and temperature ($T \propto r^{-4}$)
407 fields with distance ensures changes in the properties of the underlying rock will be very small.
408 Even with constant nominal values of thermodynamic and materials parameters, the idealized
409 model predicts a size of the region of burnt organic matter that is consistent with observations on
410 the collected samples and in the field. In the model, the temperature can theoretically reach infinity
411 at the strike point, but the lightning channel has a finite width of ~1 cm and the maximum
412 temperature is consistent with the upper limit of 10^5 K for the lightning channel (Uman, 1964).
413 The presence of barite aggregates in the fulgurite glass observed via ESEM (Fig. 4c,f) suggests
414 the possibility of post-fusion hydration and weathering by meteoric water. Newly formed barite
415 may be considered as evidence for sulfur compounds in rainwater. Vermiculite observed in Motta 5
416 via XRD (Fig. 5d) was probably formed through alteration of the fulgurite glass layer. Further
417 investigations are required to assess the relevance of lichen weathering for the bio-degradation of
418 rock fulgurite and accelerated formation of clay minerals.
419

420 **IMPLICATIONS**

421 Lightning strikes reach the ground on Earth as many as 8 million times per day or 100 times per
422 second, according to the U.S. National Severe Storms Laboratory (US-NSSL, 2017). About 90% of
423 these lightning flashes occur over continental landmasses as opposed to the open ocean (Lay et al.,
424 2007). Considering that the frequency of lightning across the globe is 1.2×10^9 flashes per year
425 (Pasek and Block, 2009), the fraction of cloud-to-ground lightning that produces a fulgurite is 0.234
426 (Pasek and Block, 2009), the rock fulgurite mass formed per strike ranges from a few 100 g to about
427 30 kg (Pasek and Block, 2009), the total mass of rock fulgurites formed worldwide is estimated to
428 be 28–8400 Mt/yr, which corresponds to an area of at least 1180 km^2/yr, assuming a density of 2.37
429 g/cm^3 (rhyolite glass, Hughes, 1982) and a thickness of rock fulgurite of 10 μm. Thus, lightning
430 affects a significant portion of the rocks exposed at the Earth's surface. Since glass is geologically

susceptible to alteration (Fisher and Schmincke, 1984; Cockell et al., 2009), the predicted large areas covered by rock fulgurites produced every year may potentially weather more rapidly than the non-affected rocks.

Fulgurites provide important information on the thermodynamic and mechanical effects of lightning on rocks. Tectonics and erosion, volcanic eruptions, flooding, weathering, glaciation, and meteorite impacts are among the processes that constantly reshape the Earth's surface over geological time. The formation of fulgurites, and the accompanying mineralogical and chemical compositional changes, may record information (*e.g.*, trapped atmospheric gas in bubbles) about the environment in which they were formed. The characteristics of a given fulgurite are extremely dependent on the particulars of each lightning strike as well as the composition of the target materials. Rock fulgurites preserve a record of the direct effects of a lightning flash, and therefore can be used to study the fine structure and physics of lightning processes. While quantitative chemical data have been acquired from rock fulgurites (*e.g.*, Essene and Fisher, 1986; Clochiatti, 1990; Grapes, 2010; Grapes and Müller-Sigmund, 2009), comparatively less information is available regarding their physical conditions of formation.

The study of rock fulgurites from Mottarone-Baveno, probed on the basis of mineralogical and compositional signatures, provides mineralogical, chemical, and physical insights into natural lightning processes (*e.g.*, disequilibrium melting, mixing, crystallization). The multi-method approach employed in this study supplies basic knowledge of fulgurite glass formation (minimum temperatures of formation, chemical variations between the host rock and glass, organic components, volatilization, porosity, and weathering) via detailed evaluation of the mineralogy, textures, and the chemical composition of both the glass and whole-rock. The XRD results constrain the minimum temperature of rock fulgurite glass formation from the mineralogical signature left by lightning when it impacted the rock. Raman spectroscopy and elemental analyzer permitted determination of the CO_x and NO_x contents, which explains the origin of the black color, a common feature of rock fulgurites. The model results allowed for estimation of the size of the region of burnt

457 organic matter, of radius ~13 cm, consistent with observations. The ESEM images reveal that voids
458 are mostly related to the degassing of burnt organic matter during the lightning event. Thus, the
459 present study contributes considerably to the evolving data-set on rock fulgurite features and
460 constrains the conditions of their formation.

461 The experimental approach taken in this paper can be applied not only to the study of fulgurite
462 glasses, but may also provide insights into other high-temperature processes in geologic systems
463 (*e.g.*, paralava formation, tektites, *etc.*) and dynamic rock transformation associated with ultrafast
464 events (*e.g.,* meteor impacts). Moreover, technical applications related to lightning effects on
465 materials may potentially benefit from the results reported in this paper. The interactions of
466 minerals and other materials with lightning are essential for mitigating thermal damage from
467 lightning strikes, the design of better lightning protection systems, and understanding the nature of
468 the lightning environment near and at the point of a direct strike.

469

470 **AKNOWLEDGEMENTS**

471 Authors would like to thank Dr. Scott Speakman, PANalytical B.V., for his valuable technical
472 advice to improve XRPD data collection. Dr. Joseph Boesenberg, Brown University, is kindly
473 acknowledged for his help in carrying out the EPMA experiments. Dr. Matthew Brukman, "Singh
474 Center for Nanotechnology" of University of Pennsylvania, is acknowledged for his assistance with
475 the Raman analyses. Prof. Alain Plante, University of Pennsylvania, is acknowledged for technical
476 advice in the use of Elemental Analyzer. Authors are grateful to the Associate Editor, Callum
477 Hetherington for his critical reading of the manuscript, helpful corrections, and additions to its
478 contents. Matthew Pasek and Kyle Ashley are kindly acknowledged for providing thoughtful and
479 constructive reviews on an earlier version of this manuscript.

480

481 **REFERENCES**

Adamo, P., Bargagli, R., Giordano, S., Modenesi, P., Monaci, F., Pittao, E., Spagnuolo, V., and Tretiach, M. (2008) Natural and pre-treatments induced variability in the chemical composition and morphology of lichens and mosses selected for active monitoring of airborne elements. Environmental Pollution, 152(1), 11-19.

Alajtal, A.I., Edwards, H.G., Elbagerma, M.A., and Scowen, I.J. (2010) The effect of laser wavelength on the Raman Spectra of phenanthrene, chrysene, and tetracene: implications for extra-terrestrial detection of polyaromatic hydrocarbons. Spectrochim Acta A Mol Biomol Spectrosc, 76(1), 1-5.

Arias, A., Oddone, M., Bigazzi, G., Di Muro, A., Principe, C., and Norelli, P. (2006) New data for the characterization of Milos obsidians. Journal of Radioanalytical and Nuclear Chemistry, 268(2), 371-386.

Boriani, A., Caironi, V., Oddone, M., and Vannucci, R. (1988) Some petrological and geochemical constraints on the genesis of Baveno Mottarone plutonic bodies. Rendiconti della Societá Italiana di Mineralogia e Petrologia, 43(2), 385-394.

Boriani, A., Giobbi Origoni, E., Borghi, A., and Caironi, V. (1990) The evolution of the “Serie dei Laghi” (Strona-Ceneri and Scisti dei Laghi): the upper component of the Ivrea-Verbano crustal section; Southern Alps, North Italy and Ticino, Switzerland. Tectonophysics, 182(1), 103-118.

Bouška, V., and Feldman, V.I. (1994) Terrestrial and Lunar, Volcanic and Impact Glasses, Tektites, and Fulgurites. In A.S. Marfunin, Ed. Advanced Mineralogy: Volume 1 Composition, Structure, and Properties of Mineral Matter: Concepts, Results, and Problems, p. 258-265. Springer Berlin Heidelberg, Berlin, Heidelberg.

Bugini, R., Pavese, A., Borroni, S., and Folli, L. (2000) White granites used in Lombard architecture. In V. Fassina, Ed. Proceedings of the 9th International Congress on Deterioration and Conservation of Stone, Venice, June 19-24, 2000, p. 41-48.

507 Caironi, V. (1985) Characterization of different granitic facies in the Baveno-Mottarone pluton.
508 Rendiconti della Societá Italiana di Mineralogia e Petrologia, 40, 341-352.
509 Carabatos-Nedelec, C. (2001) Raman Spectra of Gases. In I.R. Lewis, and H.G.M. Edwards, Eds.
510 Handbook of Raman Spectroscopy, 28, p. 423-468. CRC Press.
511 Carter, E.A., Hargreaves, M.D., Kee, T.P., Pasek, M.A., and Edwards, H.G. (2010a) A Raman
512 spectroscopic study of a fulgurite. Philos Trans A Math Phys Eng Sci, 368(1922), 3087-97.
513 Carter, E.A., Pasek, M.A., Smith, T., Kee, T.P., Hines, P., and Edwards, H.G. (2010b) Rapid
514 Raman mapping of a fulgurite. Anal Bioanal Chem, 397(7), 2647-58.
515 Christian, H.J., Blakeslee, R.J., Boccippio, D.J., Boeck, W.L., Buechler, D.E., Driscoll, K.T.,
516 Goodman, S.J., Hall, J.M., Koshak, W.J., Mach, D.M., and Stewart, M.F. (2003) Global
517 frequency and distribution of lightning as observed from space by the Optical Transient
518 Detector. Journal of Geophysical Research: Atmospheres, 108(D1).
519 Clochiatti, R. (1990) Les fulgurites et roches vitrifiées de l'Etna / Fulgurites and vitreous rocks from
520 Etna: a preliminary petrochemical study. European Journal of Mineralogy, 2(4), 479-494.
521 Cockell, C.S., Olsson-Francis, K., Herrera, A., and Meunier, A. (2009) Alteration textures in
522 terrestrial volcanic glass and the associated bacterial community. Geobiology, 7(1), 50-65.
523 Degen, T., Sadki, M., Bron, E., Konig, U., and Nenert, G. (2014) The HighScore suite. Powder
524 Diffraction, 29(SupplementS2), S13-S18.
525 Dino, G.A., Fornaro, M., and Trentin, A. (2012) Quarry Waste: Chances of a Possible Economic
526 and Environmental Valorisation of the Montorfano and Baveno Granite Disposal Sites.
527 Journal of Geological Research, 2012, 1-11.
528 Ende, M., Schorr, S., Kloess, G., Franz, A., and Tovar, M. (2012) Shocked quartz in Sahara
529 fulgurite. European Journal of Mineralogy, 24(3), 499-507.
530 Eppelbaum, L., Kutasov, I., and Pilchin, A. (2014) Thermal properties of rocks and density of
531 fluids. In L. Eppelbaum, I. Kutasov, and A. Pilchin, Eds. Applied geothermics, p. 99-149.
532 Springer-Verlag (Lecture Notes in Earth System Sciences) Berlin Heidelberg.

533 Essene, E.J., and Fisher, D.C. (1986) Lightning strike fusion: extreme reduction and metal-silicate
534 liquid immiscibility. Science, 234(4773), 189-93.
535 Fisher, R.V., and Schmincke, H.-U. (1984) Alteration of Volcanic Glass. In R.V. Fisher, and H.-U.
536 Schmincke, Eds. Pyroclastic Rocks, p. 312-345. Springer Berlin Heidelberg, Berlin,
537 Heidelberg.
538 Frederikse, H.P.R. (2004) Section 12: Properties of solids. Thermal conductivity of ceramics and
539 other insulating materials. In D.R. Lide, Ed. Handbook of Chemistry and Physics. 84th
540 edition, p. 12-227. CRC Press.
541 French, B.M., and Koeberl, C. (2010) The convincing identification of terrestrial meteorite impact
542 structures: What works, what doesn't, and why. Earth-Science Reviews, 98(1-2), 123-170.
543 Frost, B.R., Barnes, C.G., Collins, W.J., Arculus, R.J., Ellis, D.J., and Frost, C.D. (2001) A
544 geochemical classification for granitic rocks. Journal of Petrology, 42(11), 2033-2048.
545 Gallitelli, P. (1937) Ricerche petrografiche sul granito di Baveno. Memorie della Societá Toscana di
546 Scienze Naturali, 46, 150-226.
547 Garra, P., Maschowski, C., Liaud, C., Dieterlen, A., Trouve, G., Le Calve, S., Jaffrezo, J.L.,
548 Leyssens, G., Schonnenbeck, C., Kohler, S., and Gieré, R. (2015) Fluorescence Microscopy
549 Analysis of Particulate Matter from Biomass Burning: Polyaromatic Hydrocarbons as Main
550 Contributors. Aerosol Science and Technology, 49(11), 1160-1169.
551 Gieré, R., Wimmenauer, W., Muller-Sigmund, H., Wirth, R., Lumpkin, G.R., and Smith, K.L.
552 (2015) Lightning-induced shock lamellae in quartz. American Mineralogist, 100(7), 1645-
553 1648.
554 Grapes, R. (2010) Thermal Regimes and Effects. In R. Grapes, Ed. Pyrometamorphism, p. 11-44.
555 Springer Berlin Heidelberg, Berlin, Heidelberg.
556 Grapes, R.H., and Müller-Sigmund, H. (2009) Lightning-strike fusion of gabbro and formation of
557 magnetite-bearing fulgurite, Cornone di Blumone, Adamello, Western Alps, Italy.
558 Mineralogy and Petrology, 99(1-2), 67-74.

559 Holland, T., and Powell, R. (2001) Calculation of phase relations involving haplogranitic melts
560 using an internally consistent thermodynamic dataset. Journal of Petrology, 42(4), 673-683.
561 Hughes, C.J. (1982) Physical properties and physical chemistry of magmas. In C.J. Hughes, Ed.
562 Igneous Petrology, 7, p. 147-198. Elsevier.
563 Jager, E., and Faul, H. (1959) Age measurements on some granites and gneisses from the Alps
564 Geological Society of America Bulletin, 70(12), 1553-1558.
565 Kenkmann, T., Poelchau, M.H., and Wulf, G. (2014) Structural geology of impact craters. Journal
566 of Structural Geology, 62, 156-182.
567 Lay, E.H., Jacobson, A.R., Holzworth, R.H., Rodger, C.J., and Dowden, R.L. (2007) Local time
568 variation in land/ocean lightning flash density as measured by the World Wide Lightning
569 Location Network. Journal of Geophysical Research-Atmospheres, 112(D13), D13111-
570 D13120.
571 Martin Crespo, T., Lozano Fernandez, R.P., and Gonzalez Laguna, R. (2009) The fulgurite of Torre
572 de Moncorvo (Portugal): description and analysis of the glass. European Journal of
573 Mineralogy, 21(4), 783-794.
574 Navarro-Gonzalez, R., Mahan, S.A., Singhvi, A.K., Navarro-Aceves, R., Rajot, J.L., McKay, C.P.,
575 Coll, P., and Raulin, F. (2007) Paleoecology reconstruction from trapped gases in a fulgurite
576 from the late Pleistocene of the Libyan Desert. Geology, 35(2), 171-174.
577 O'Connor, B.H., and Raven, M.D. (1988) Application of the Rietveld Refinement Procedure in
578 Assaying Powdered Mixtures. Powder Diffraction, 3(01), 2-6.
579 O'Dwyer, J.J. (1969) Theory of Dielectric Breakdown in Solids. Journal of The Electrochemical
580 Society, 116(2), 239-242.
581 Olhoeft, G.R. (1981) Electrical properties of granite with implications for the lower crust. Journal of
582 Geophysical Research: Solid Earth, 86(B2), 931-936.

583 Olona, J., Pulgar, J., Fernández-Viejo, G., López-Fernández, C., and González-Cortina, J. (2010)
584 Weathering variations in a granitic massif and related geotechnical properties through
585 seismic and electrical resistivity methods. Near Surface Geophysics, 8(1750), 585-599.
586 Pasek, M., and Block, K. (2009) Lightning-induced reduction of phosphorus oxidation state. Nature
587 Geoscience, 2(8), 553-556.
588 Pasek, M.A., Block, K., and Pasek, V. (2012) Fulgurite morphology: a classification scheme and
589 clues to formation. Contributions to Mineralogy and Petrology, 164(3), 477-492.
590 Pasek, M.A., and Hurst, M. (2016) A Fossilized Energy Distribution of Lightning. Scientific
591 Reports, 6, 30586.
592 Pouchou, J.-L., and Pichoir, F. (1991) Quantitative Analysis of Homogeneous or Stratified
593 Microvolumes Applying the Model "PAP". In K.F.J. Heinrich, and D.E. Newbury, Eds.
594 Electron Probe Quantitation, p. 31-75. Springer US, Boston, MA.
595 Rakov, V.A. (1999) Lightning makes glass. 29th Annual Conference of the Glass Art Society p. 45-
596 50, Tampa, Florida.
597 Saikia, B.J., Parthasarathy, G., Sarmah, N.C., and Baruah, G.D. (2008) Fourier-transform infrared
598 spectroscopic characterization of naturally occurring glassy fulgurites. Bulletin of Materials
599 Science, 31(2), 155-158.
600 Sandrone, R., Colombo, A., Fiora, L., Fornaro, M., Lovera, E., Tunesi, A., and Cavallo, A. (2004)
601 Contemporary natural stones from the Italian western Alps. Periodico di Mineralogia,
602 73(SPECIAL ISSUE 3: A showcase of the Italian research in applied petrology), 211-226.
603 Schneider, C.A., Rasband, W.S., and Eliceiri, K.W. (2012) NIH Image to ImageJ: 25 years of image
604 analysis. Nat Methods, 9(7), 671-5.
605 Sinigoi, S., Quick, J.E., Demarchi, G., and Klötzli, U.S. (2016) Production of hybrid granitic
606 magma at the advancing front of basaltic underplating: Inferences from the Sesia Magmatic
607 System (south-western Alps, Italy). Lithos, 252–253, 109-122.

608 Socrates, G. (2001) Infrared and Raman Characteristic Group Frequencies: Tables and Charts, 3rd
609 Edition. Wiley.
610 Sponholz, B. (2004) Fulgurites as palaeoclimatic indicators - the proof of fulgurite fragments in
611 sand samples. In W. Smykatz-Kloss, and P. Felix-Henningsen, Eds. Paleoecology of
612 Quaternary Drylands, p. 73-78. Springer Berlin Heidelberg, Berlin, Heidelberg.
613 Sponholz, B., Baumhauer, R., and Felix-Henningsen, P. (1993) Fulgurites in the southern Central
614 Sahara, Republic of Niger and their palaeoenvironmental significance. The Holocene, 3(2),
615 97-104.
616 Switzer, G., and Melson, W.G. (1972) Origin and composition of rock fulgurite glass. The Earth
617 Scientist 9.
618 Uman, M.A. (1964) The peak temperature of lightning. Journal of Atmospheric and Terrestrial
619 Physics, 26(1), 123-128.
620 Uman, M.A. (1969) Lightning. 264 p. McGraw-Hill, NY.
621 Uman, M.A., and Krider, E.P. (1989a) Natural and Artificially Initiated Lightning. Science, New
622 Series, 246(4929), 457-464.
623 Uman, M.A., and Krider, E.P. (1989b) Natural and Artificially Initiated Lightning. Science,
624 246(4929), 457-464.
625 US-NSSL. (2017) U.S. National Severe Storms Laboratory. Available:
626 http://www.nssl.noaa.gov/research/lightning/ (accessed February 22, 2017)
627 White, R.H., and Dietenberger, M.A. (2001) Wood products: thermal degradation and fire. In C.R.
628 K. H. Buschow J, Flemings MC, Ilschner B, Kramer EJ, Mahajan S, Veyssière P, Ed.
629 Encyclopedia of materials: science and technology, p. 9712-9716. Elsevier Science Ltd.
630 Zingg, A. (1983) The Ivrea and Strona-Ceneri zones (southern Alps, Ticino and N- Italy) - a review.
631 Schweizerische Mineralogische und Petrographische Mitteilungen, 63(2-3), 361-392.

632

633 **Figure Captions**

634 **Fig. 1** The samples studies were collected near the top of Mt. Mottarone, Italy from a well-exposed,
635 N–S trending ridge, which forms steep cliffs (a). The rock fulgurite from Mt. Mottarone
636 appears as a dark brown-black layer on the surface of the granite, known as pink Baveno
637 granite. Hammer for scale. Circles show the presence of lichen and algal biofilms on the
638 pink granite in close vicinity of the site where the fulgurite samples have been recovered (b).

639 **Fig. 2** X-ray diffraction pattern of the bulk granite (sample Motta 6). Observed spectra (red line),
640 fitted spectra (blue solid line), and Bragg peak positions (tick marks above difference plot)
641 are shown. Qtz = quartz; Plg = plagioclase; Ksp = K-feldspar; Bio = biotite.

642 **Fig. 3** Plane-polarized light image of a finely cracked quartz crystal located immediately below the
643 fulgurite layer, which appears as dark rim.

644 **Fig. 4** Microscopic images of the rock fulgurite from Mt. Mottarone, Italy. (a) Cross-polarized light
645 image of brown-black glassy fulgurite layer coating Baveno granite. (b) Plane-polarized
646 light image of a glassy fulgurite layer coating potassium feldspar and containing opaque
647 spheres (FeO-SiO_2-rich). BSE images of (c) fulgurite layer of Motta 5 containing FeO-SiO_2-
648 rich spheres, which appear as small, round objects with a very bright contrast; (d) fulgurite
649 glass of Motta 7; e) distinctly porous fulgurite layer in contact with a potassium feldspar
650 crystal in Motta 5; and (f) porous fulgurite layer in contact with cracked quartz crystal,
651 which forms the substrate in Motta 5. The tiny bright spots in the fulgurite were determined
652 to be barite by ESEM-EDS. A flow-banding texture is observed in the upper part of
653 fulgurite layer. Pores sizes are highly variables in the fulgurite glass: micro-vesicles are
654 mostly distributed along the top of the fulgurite, whereas larger pores are observed at the
655 boundary of the substrate. Qtz = quartz; Plg =plagioclase; Ksp = K-feldspar; Bio = biotite;
656 Brt = barite.

657 **Fig. 5** X-ray diffraction patterns of the studied rock fulgurite. Rietveld method with K-factor
658 approach profile fitting of fulgurite samples (a) Motta 2, (b) Motta 3, (c) Motta 4, (d) Motta

5, (e) Motta 6, (f) Motta 7. Observed spectra (red line), fitted spectra (blue solid line), and Bragg peak positions (tick marks above difference plot) are shown. Ver = vermiculite; Plg = plagioclase; Qtz = quartz; Cris = cristobalite.

Fig. 6 Secondary electron images of a partially melted biotite crystal. The crystal was detected by optical microscopy at the boundary between the granite substrate and the fulgurite layer. (a) overview of partially melted crystal surface; (b) Detail of melted top layers of biotite.

Fig. 7 Correlation between quantity of carbon (up to 7 wt%, expressed as CO_x) and nitrogen (up to 0.87 wt%, expressed as NO_x) species in the fulgurite glass of various samples from Mt. Mottarone. Data from Table 7.

Fig. 8 Micro-Raman spectra of polyaromatic hydrocarbon molecules, monomer SiO_4 units, and cristobalite microlites in the fulgurite layer of sample Motta 7. The Raman spectra were collected in four different areas of the layer, at the same experimental conditions. (a) *cis*-isomer of vinylene hydrocarbon compounds *cis*–CH=CH– (853 cm^{-1}), oxime group >C=N– (1470 cm^{-1}), and alkene C=C conjugated with –N (1633 cm^{-1}). (b) alkene C=C conjugated to an aromatic group (540 cm^{-1}), scattering of cristobalite microlites (780 cm^{-1}), and monomer SiO_4 units (836 cm^{-1}); (c) vinylidenes hydrocarbon functional group >C=CH_2 (1402 cm^{-1}) and alkene C=C conjugated to an aromatic group and to cyclic alkenes (1622 cm^{-1}); (d) C–C stretching (1357 cm^{-1}) and alkene C=C conjugated with –N (1633 cm^{-1}). The broad peaks at 2030 and 2300 cm^{-1} in all spectra are consistent with water molecules in the glass matrix.

Fig. 9 Modeling results showing the radial distributions of the electrical field (blue curve) and the temperature (red curve). The maximum temperature is truncated to remove the singularities at $r = 0$. The dashed horizontal line shows the temperature at which the organic matter starts to burn (300 °C). The effect of Joule heating is shown to be strongest near the lightning hit point (at $r = 0$), and the burnt region extends to about 13 cm.

Table 1 Mineralogical composition of the bulk-rock granite samples from Baveno, Italy. Concentrations in wt%, as determined by Rietveld analysis.

Weight %	Motta 2	Motta 3	Motta 4	Motta 5	Motta 6	Motta 7
Quartz	72.3(3)	71.2(5)	61.4(2)	55.9(3)	67.9(2)	63.1(2)
Plagioclase	15.6(5)	10.7(6)	23.1(7)	18.1(1)	13.7(4)	29.4(7)
K-feldspar	8.7(3)	13.8(3)	2.78(2)	21.1(2)	13.3(2)	0.6(5)
Biotite	3.49(3)	3.6(2)	11.2(4)	4.8(8)	5.1(2)	6.9(3)
Chlorite		0.7(3)*	1.5(4)*			

Standard deviation in parenthesis

* At or near the detection limit (1 wt%).

Table 2 Chemical composition (wt%) of the granite from the fulgurite site at Mt. Mottarone, Italy determined using X-ray fluorescence (XRF).

	Concentration
SiO_2	77.4
Al_2O_3	12.7
Fe_2O_3 (tot)	1.15
MgO	0.12
CaO	0.12
K_2O	4.85
Na_2O	3.25
TiO_2	0.05
MnO	0.02
P_2O_5	<0.01
Cr_2O_3	0.02
V_2O_5	<0.01
BaO	<0.01
ZrO	<0.01
Cu	<0.01
Zn	<0.01
S	<0.01
LOI (loss on ignition)	1.15
∑	100.9

Detection limit 0.01 wt%

Table 3 Chemical composition (EPMA data) of plagioclase and orthoclase in the granite from the fulgurite site on Mt. Mottarone.

	Plagioclase	Orthoclase		Plagioclase	Orthoclase
	wt%			apfu (based on 5 cations)	
n	**6**	**6**			
SiO_2	68.15(0.2)	64.53(0.2)	Si	2.946	2.989
TiO_2	<0.01	<0.01	Ti	-	-
Al_2O_3	19.83(0.2)	18.45(0.2)	Al	1.010	1.007
FeO(tot)	0.06(0.01)	0.03(0.01)	Fe^{2+}	0.002	0.001
MgO	<0.01	<0.01	Mg	-	-
CaO	0.23(0.1)	<0.01	Ca	0.011	-
Na_2O	12.11(0.2)	0.53(0.4)	Na	1.015	0.047
K_2O	0.27(0.2)	16.17(0.4)	K	0.015	0.956
BaO	<0.01	<0.01	Ba	-	-
Σ	100.67	99.71			
				End-member proportions (mol%)	
			An	1.02	0
			Ab	97.55	4.70
			Or	1.43	95.30

Standard deviation in parenthesis.
n = number of data points.

Table 4 Crystalline and amorphous components (wt%, as determined by Rietveld analysis) of fulgurite samples. With the exception of values <1 wt%, all values have been rounded to the nearest unit.

K-Factor Corrected Weight %	Motta 2	Motta 3	Motta 4	Motta 5	Motta 6	Motta 7
Quartz	2.0 (3)	1.4(2)	14.1(1)	16.2(3)	11.0(1)	7.6(2)
Cristobalite		0.5(4)*	5.0(2)	1.1(2)	1.0(2)	0.2(1)*
Vermiculite				0.4(7)*		
Albite				15.8(2)	13.0(2)	14.0(1)
Amorphous	98.0(4)	98.1(2)	81.0(3)	66.6(3)	76.1(3)	78.0(1)

Standard deviation in parenthesis.

* At or near the detection limit.

Table 5 Chemical composition of fulgurite glass (EPMA data, in wt%) on selected samples.

	Motta 5	Motta 6	Motta 7
n	**8**	**10**	**10**
Na_2O	0.04(0.1)	0.04(0.1)	0.07(0.1)
SiO_2	71.97(1)	75.79(1)	73.93(1)
MgO	0.20(0.2)	0.26(0.02)	0.25(0.2)
Al_2O_3	7.79(1)	7.54(0.1)	7.76(1)
P_2O_5	0.19(0.02)	0.50(0.2)	0.07(0.1)
SO_3	0.22(0.2)	0.43(0.1)	0.44(0.3)
K_2O	0.12(0.1)	0.21(0.1)	0.28(0.3)
CaO	0.82(1)	0.83(0.1)	0.75(1)
TiO_2	0.03(0.01)	0.05(0.01)	0.04(0.1)
MnO	0.02(0.01)	0.05(0.1)	0.10(0.1)
FeO(tot)	0.22(0.2)	0.51(0.2)	0.41(1)
NiO	<0.01	0.02(0.01)	0.02(0.01)
BaO	0.04(0.1)	0.03(0.1)	0.03(0.01)
F	0.02(0.01)	0.01(0.01)	0.84(1)
∑	81.66	86.25	87.27

Standard deviation in parenthesis.
n = number of data points.

Table 6 Total organic matter analyses (wt%) of fulgurite layer.

Oxide	Motta 2	Motta 3	Motta 4	Motta 5	Motta 6	Motta 7
NO_x	0.42	0.35	0.57	0.87	0.45	0.75
CO_x	2.27	2.13	4.47	6.99	2.60	4.49
N/C	1/5	1/6	1/8	1/8	1/5	1/5

uncertainties are approximately ±0.02 wt%

Figure 1

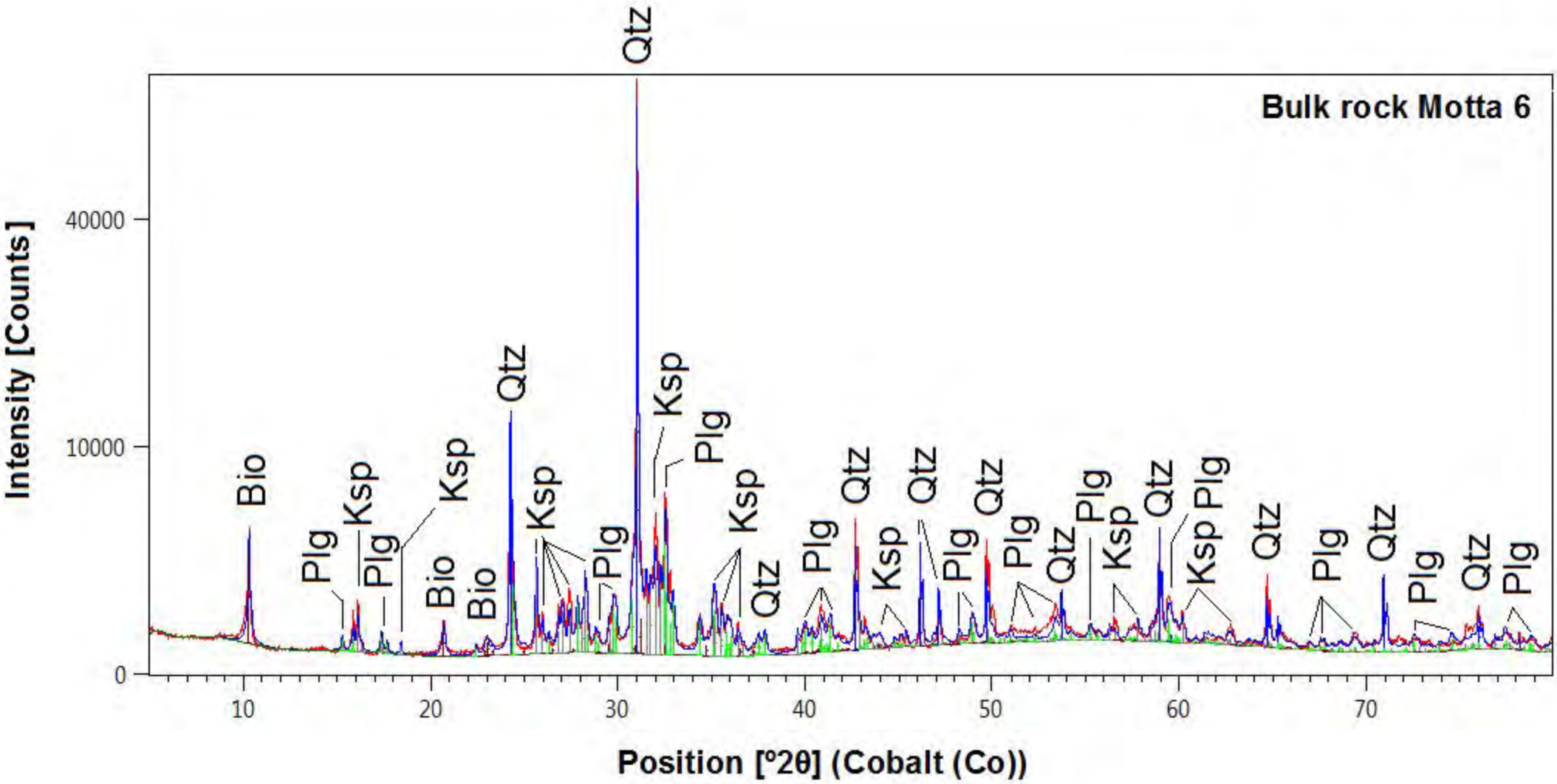
Bulk rock Motta 6
Intensity [Counts]
40000
10000
0
10
20
30
40
50
60
70
Position [°2θ] (Cobalt (Co))
Qtz
Bio
Plg
Ksp
Plg
Ksp
Bio
Bio
Qtz
Ksp
Plg
Qtz
Ksp
Plg
Ksp
Qtz
Plg
Qtz
Ksp
Qtz
Plg
Qtz
Plg
Qtz
Plg
Ksp
Qtz
Ksp
Plg
Qtz
Plg
Qtz
Plg

Figure 2

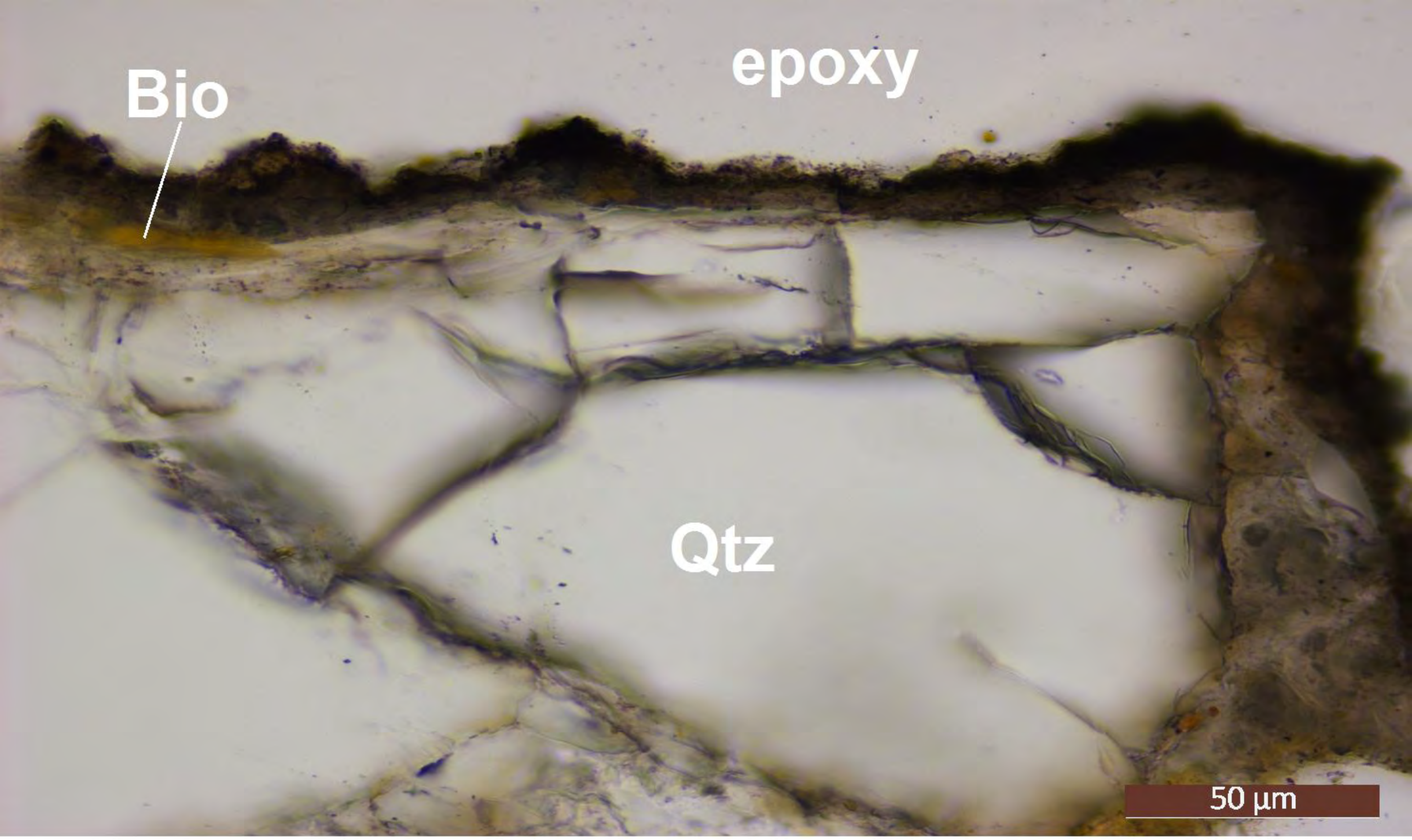

Figure 3

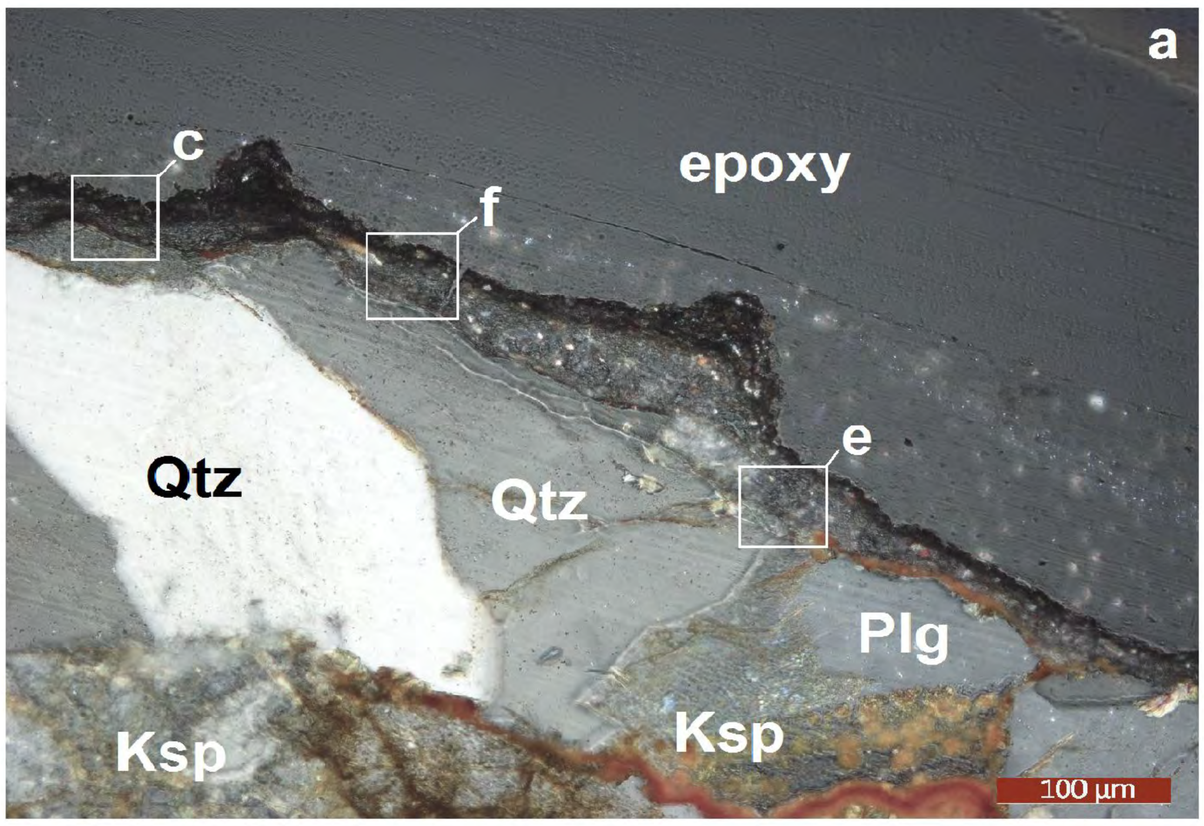
a
c
f
e
epoxy
Qtz
Qtz
Plg
Ksp
Ksp
100 µm

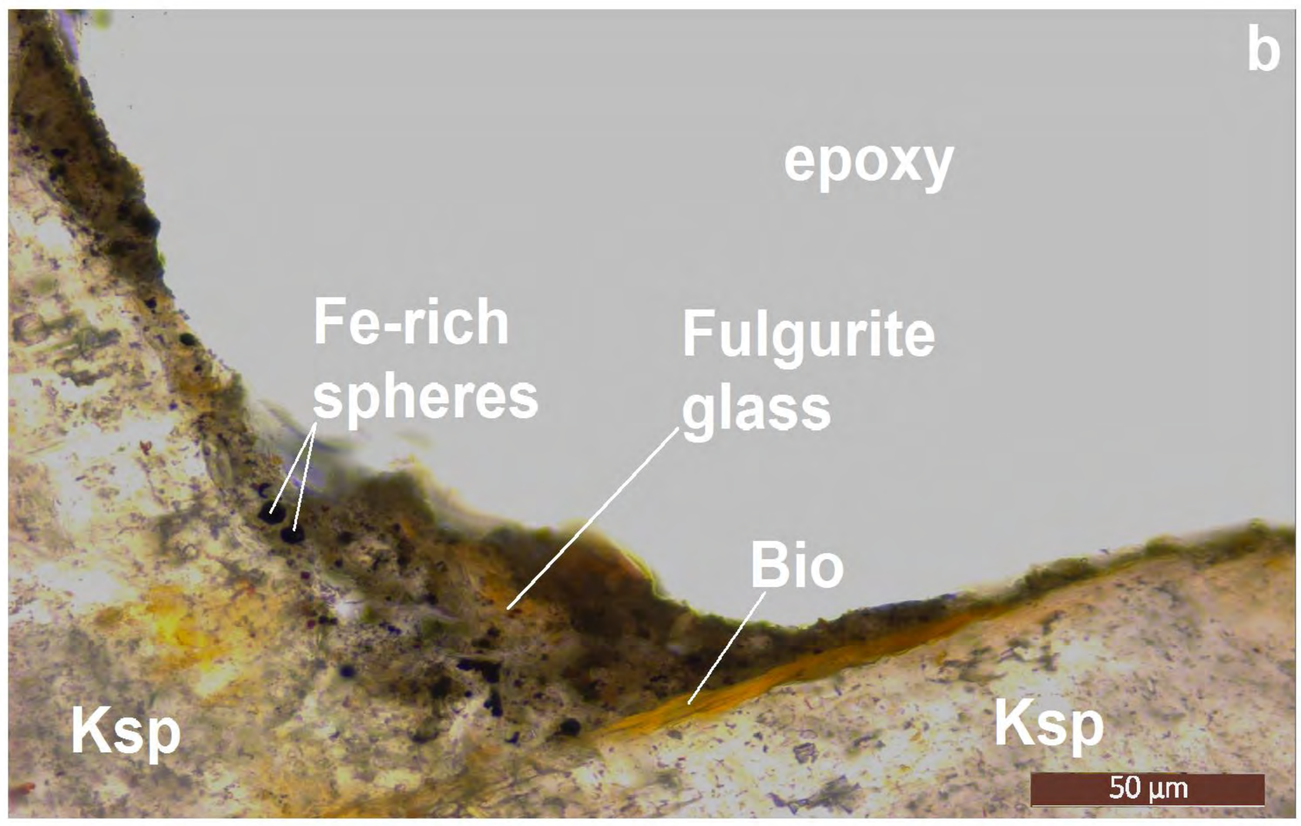
b
epoxy
Fe-rich spheres
Fulgurite glass
Bio
Ksp
Ksp
50 µm


c
Plg
Brt
Fe-rich spheres
Qtz
epoxy
Fe-rich spheres
Brt
Qtz
Plg
Brt
Qtz
2/9/2016 4:57:53 PM
mag 4 254 x
HV 15.00 kV
WD 10.7 mm
spot 5.0
mode Z Cont
20 µm


d
epoxy
Fe-rich spheres
Plg
Qtz
Plg
Brt
Qtz
4/8/2016 3:35:05 PM
mag 5 382 x
HV 10.00 kV
WD 9.8 mm
spot 3.0
mode Z Cont
10 µm

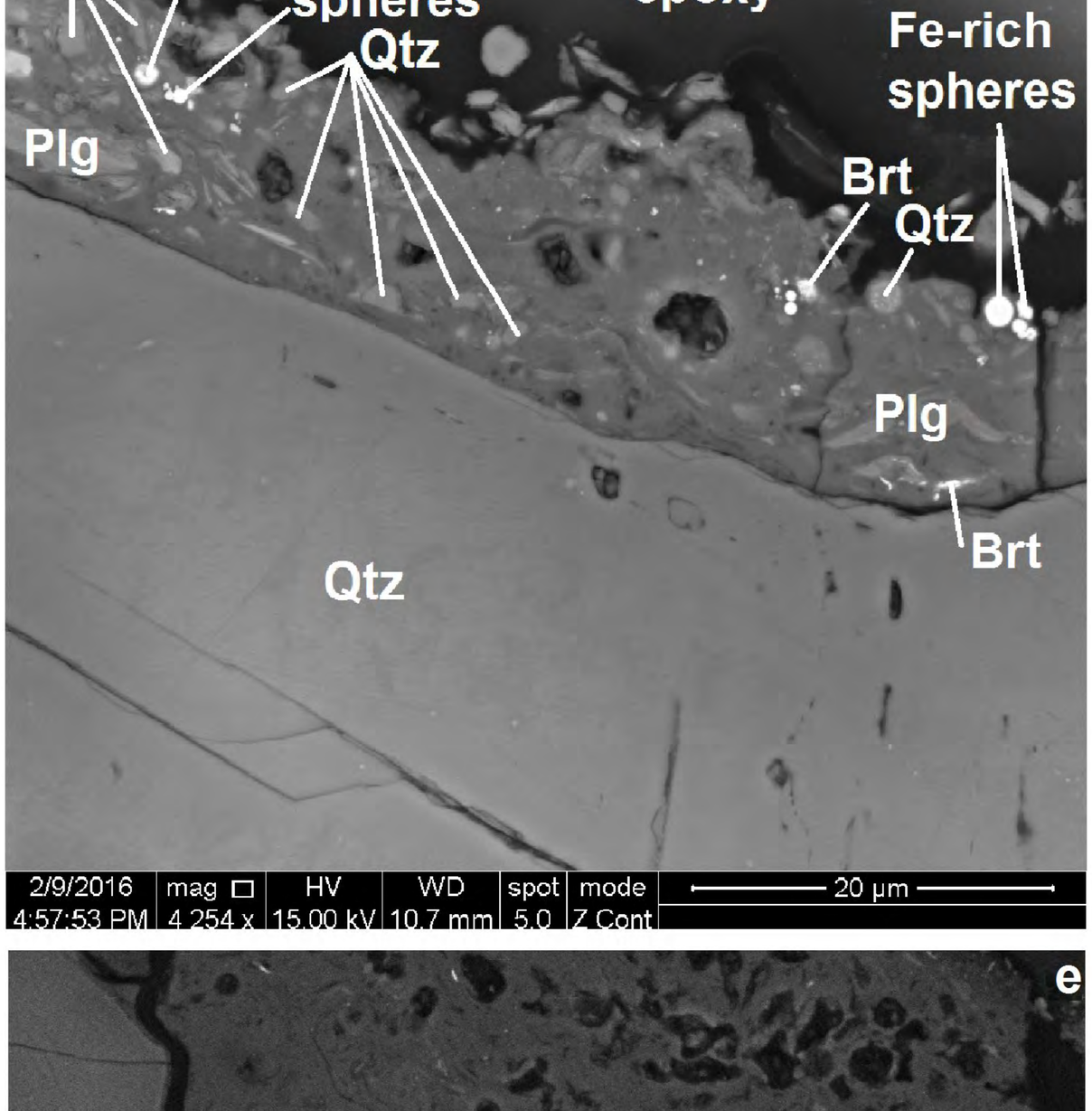
e
Plg
Ksp
Qtz
Ksp
2/25/2016 10:15:36 AM
mag 3 353 x
HV 10.00 kV
WD 10.2 mm
spot 3.0
mode Z Cont
20 µm

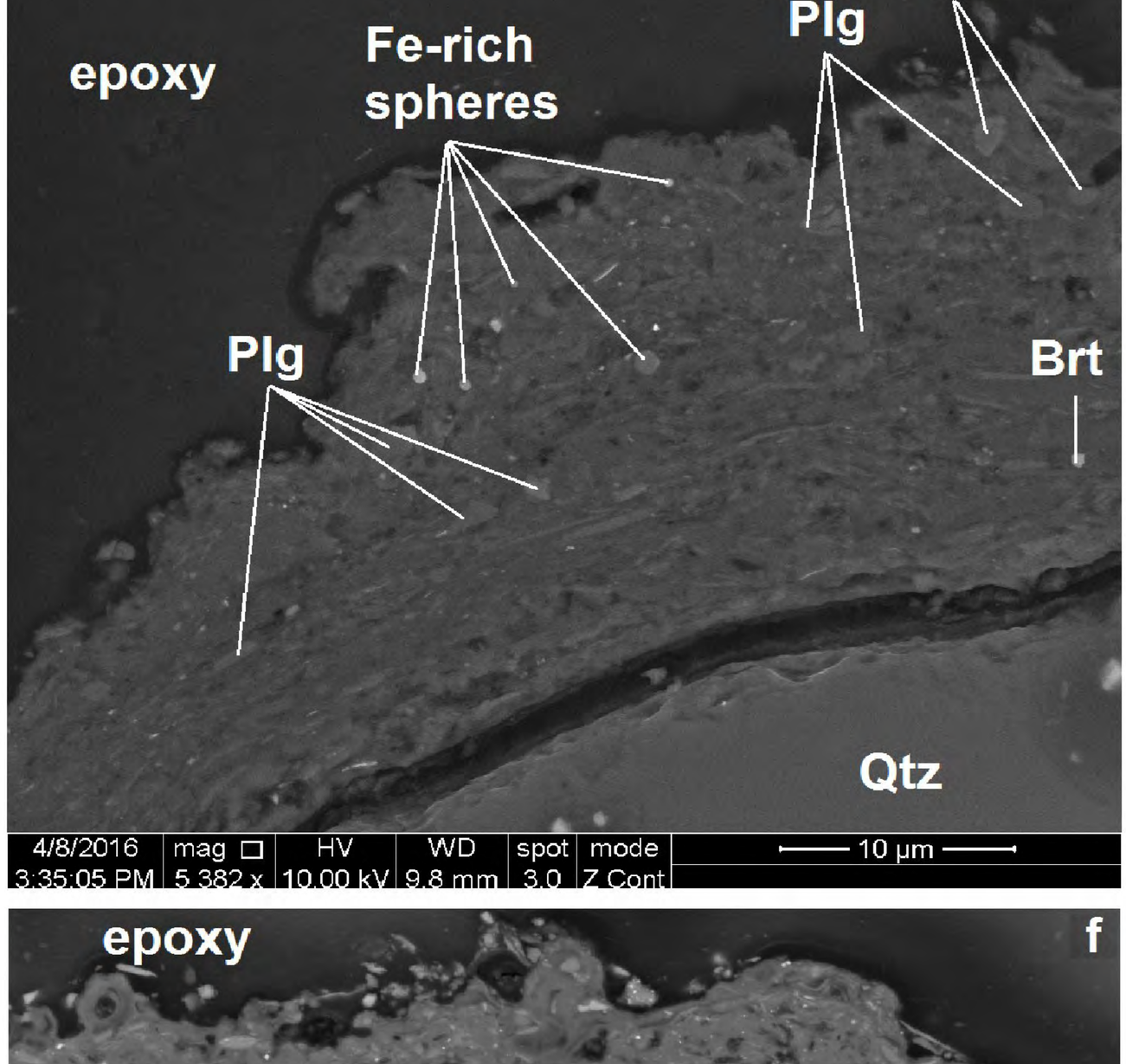
epoxy
f
Brt
Plg
Qtz
Brt
Qtz
2/9/2016 5:07:45 PM
mag 3 008 x
HV 15.00 kV
WD 10.7 mm
spot 5.0
mode Z Cont
30 µm

Figure 4

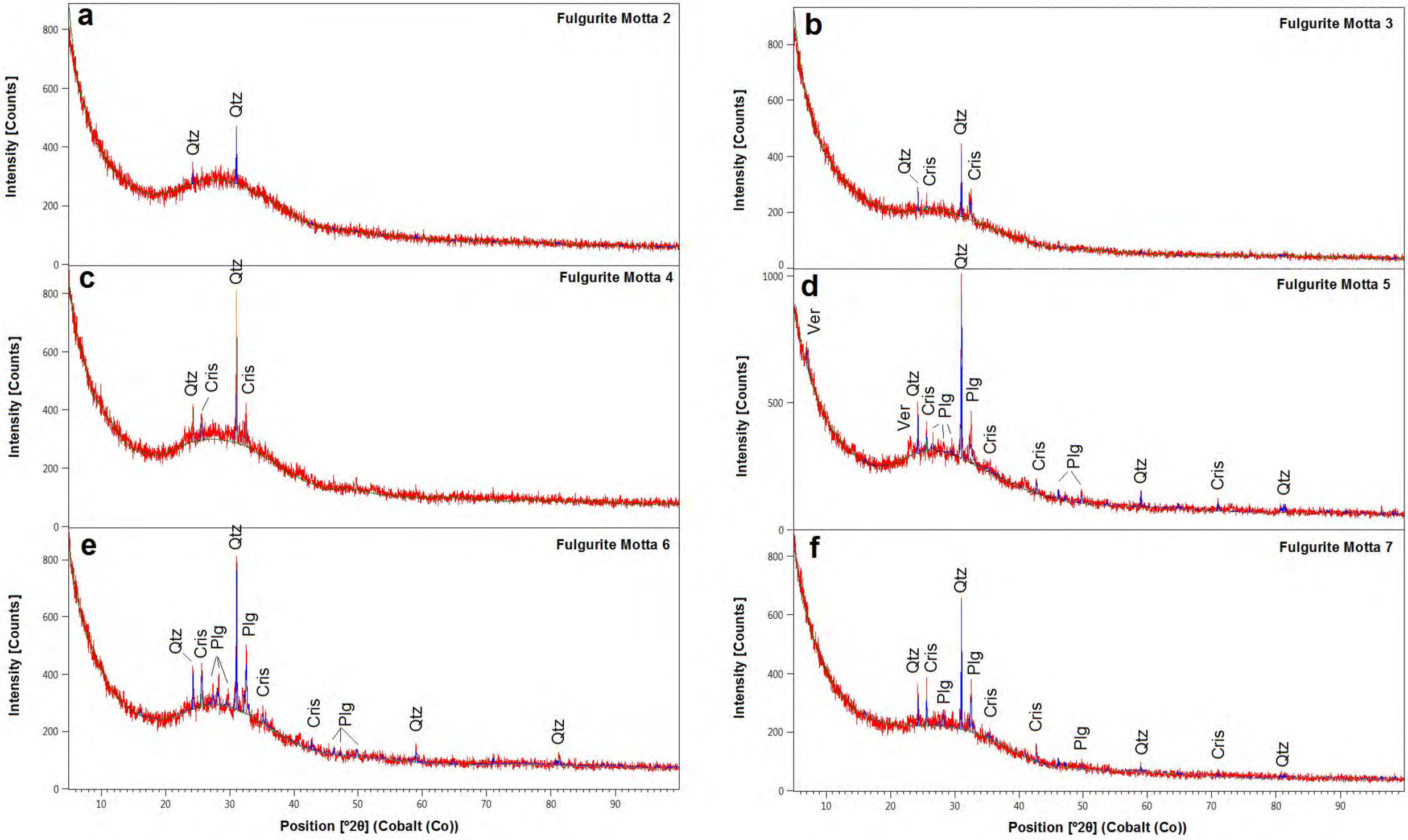
a
Fulgurite Motta 2
b
Fulgurite Motta 3
c
Fulgurite Motta 4
d
Fulgurite Motta 5
e
Fulgurite Motta 6
f
Fulgurite Motta 7
Intensity [Counts]
Position [°2θ] (Cobalt (Co))
Qtz
Cris
Plg
Ver

Figure 5

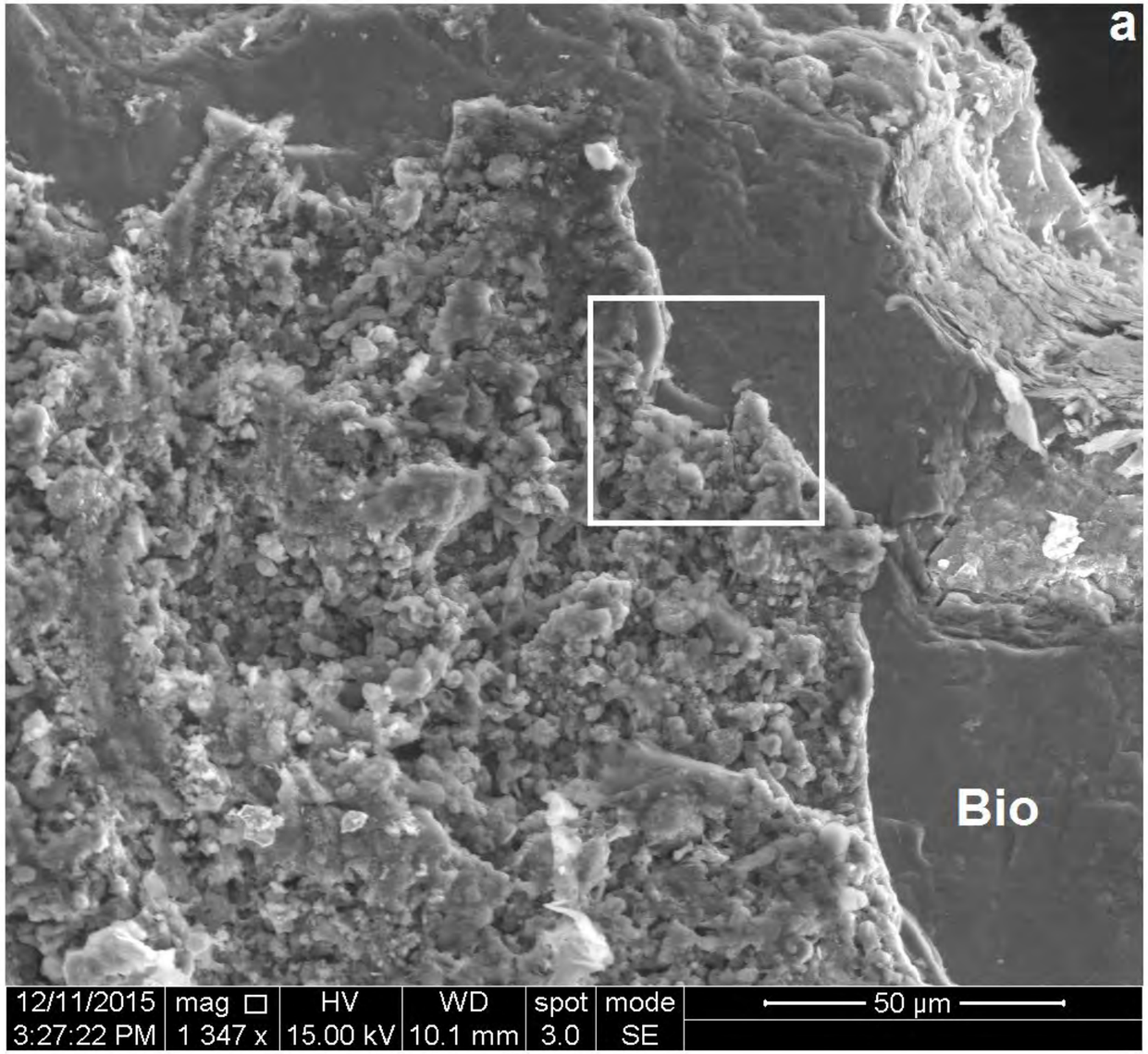
a
Bio
12/11/2015
3:27:22 PM
mag
1 347 x
HV
15.00 kV
WD
10.1 mm
spot
3.0
mode
SE
50 µm

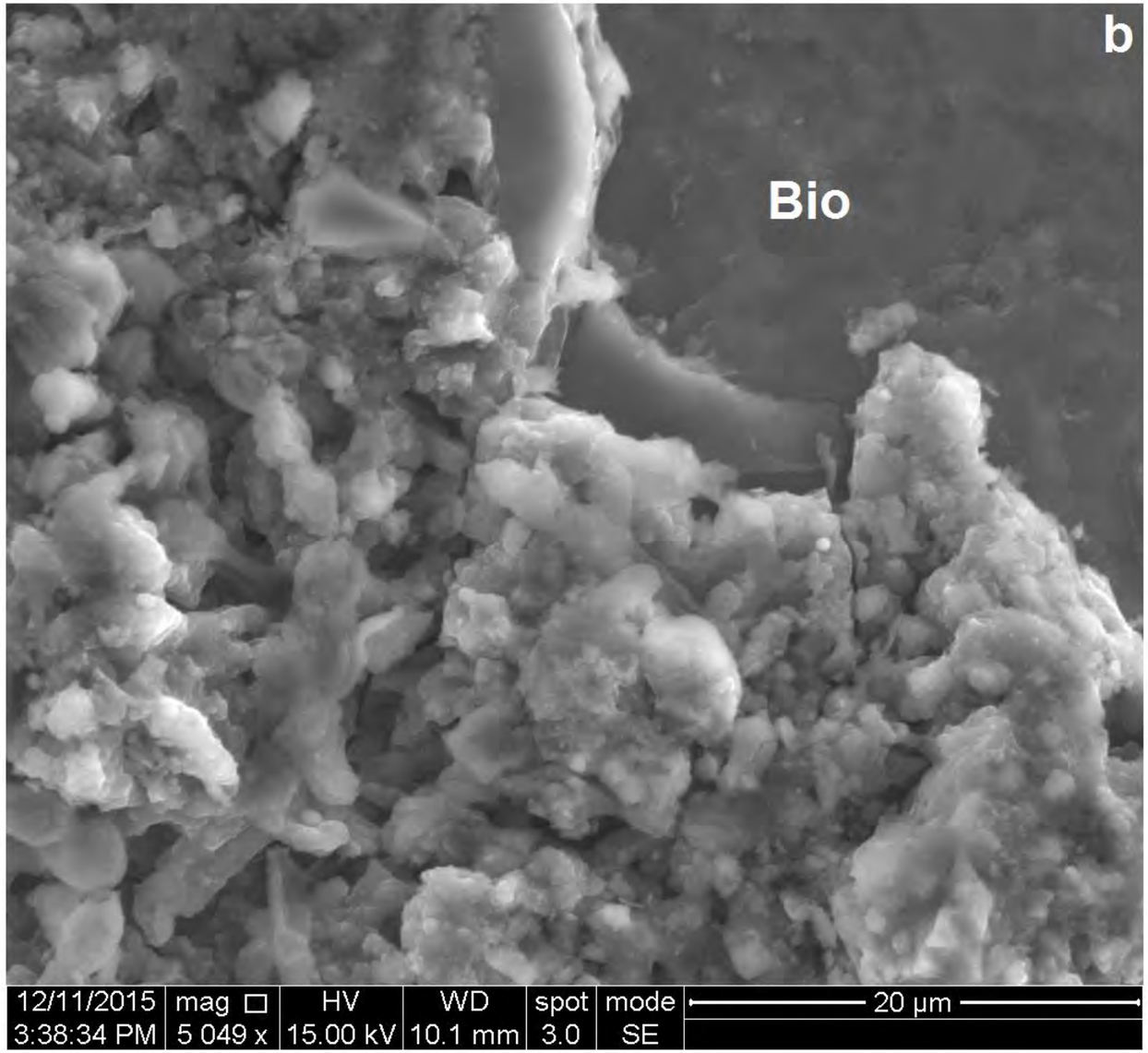
b
Bio
12/11/2015
3:38:34 PM
mag
5 049 x
HV
15.00 kV
WD
10.1 mm
spot
3.0
mode
SE
20 µm

Figure 6

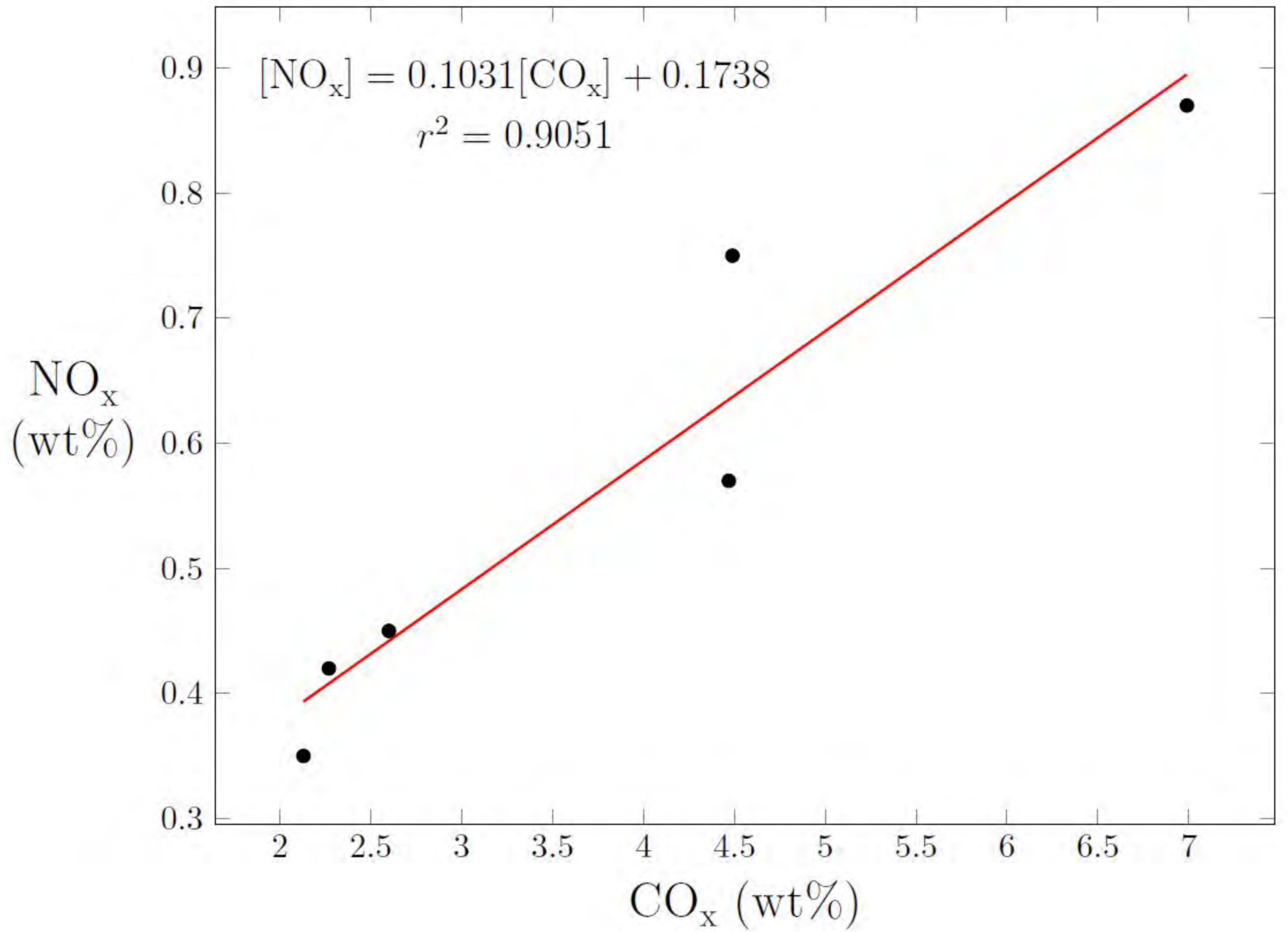
$[NO_x] = 0.1031[CO_x] + 0.1738$
$r^2 = 0.9051$
NO_x (wt%)
CO_x (wt%)
0.9
0.8
0.7
0.6
0.5
0.4
0.3
2
2.5
3
3.5
4
4.5
5
5.5
6
6.5
7

Figure 7

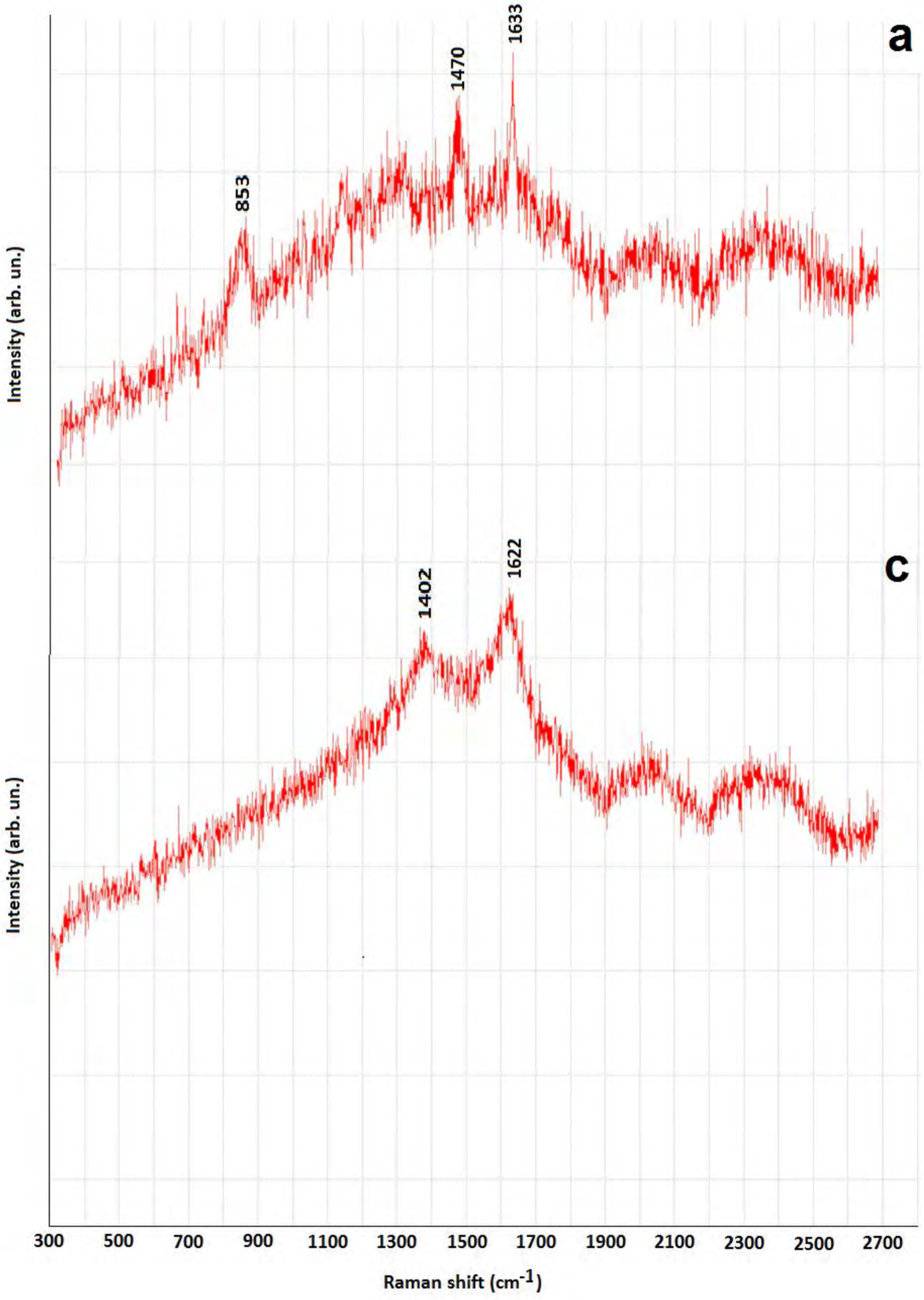
a
853
1470
1633
Intensity (arb. un.)
b
540
780
836
Intensity (arb. un.)
c
1402
1622
Intensity (arb. un.)
d
1357
1633
Intensity (arb. un.)
300
500
700
900
1100
1300
1500
1700
1900
2100
2300
2500
2700
Raman shift (cm-1)

Figure 8

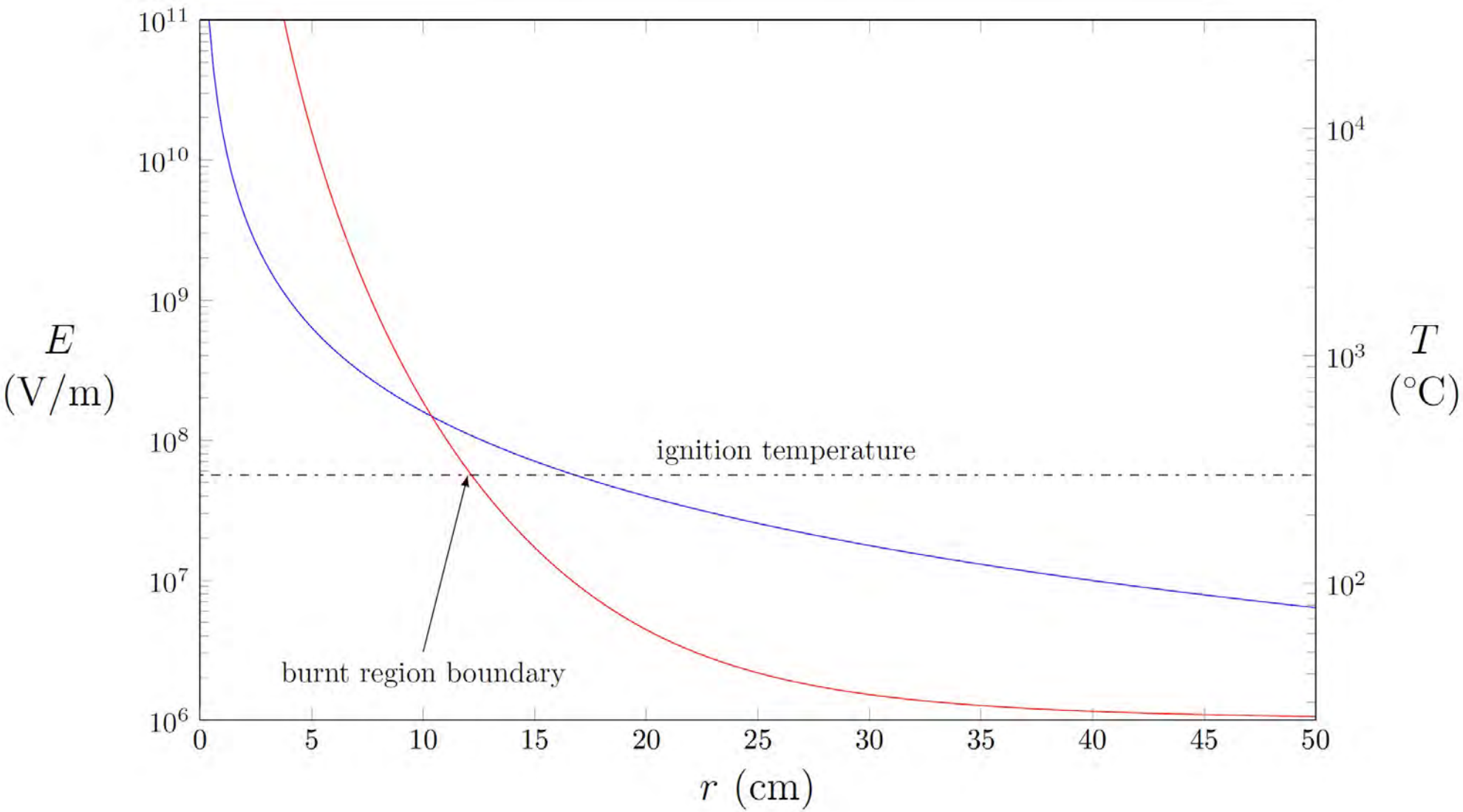
10^{11}
10^{10}
10^{9}
10^{8}
10^{7}
10^{6}
E (V/m)
10^{4}
10^{3}
10^{2}
T (°C)
ignition temperature
burnt region boundary
0
5
10
15
20
25
30
35
40
45
50
r (cm)

Figure 9